Palaeoecology of Middle Miocene charophytes from the Vallès–Penedès and Vilanova basins (Catalonia, Spain)

Josep Sanjuan[1,2*], Damià Matamoros[3], Isaac Casanovas-Vilar[4], Alba Vicente[1,2,5], Josep Anton Moreno-Bedmar[6], Jonathan Holmes[7], Carles Martín-Closas[1,2]

[1] Departament de Dinàmica de la Terra i de l'Oceà, Facultat de Ciències de la Terra, Universitat de Barcelona-UB, 08028 Barcelona, Catalonia (Spain)

[2] Institut de Recerca de la Biodiversitat (IRBio). Universitat de Barcelona-UB, 08028 Barcelona, Catalonia (Spain)

[3] Dianastrasse 10a, 9200 Gossau SG, Switzerland

[4] Institut Català de Paleontologia Miquel Crusafont, Universitat Autònoma de Barcelona, Edifici ICTA-ICP, c/Columnes s/n, Campus de la UAB, 08193 Cerdanyola del Vallès, Barcelona, Catalonia (Spain)

[5] Instituto Politécnico Nacional. Av. IPN s/N, Col. Playa Palo de Santa Rita. C.P. 23096, La Paz, BCS, Mexico

[6] Instituto de Geología, Universidad Nacional Autónoma de México, Ciudad Universitaria, Coyoacán, 04510, Ciudad de México, Mexico

[7] Environmental Change Research Centre, Department of Geography, University College London, London WC1E 6BT, United Kingdom

*Corresponding author: josepsanjuan@ub.edu

Abstract

A diverse charophyte assemblage from the Early-Middle Miocene of the Vallès–Penedès and Vilanova basins (Catalonia, NE Spain) is here described and illustrated for the first time. This flora has been recovered from three localities: els Casots (Subirats), Vilobí del Penedès, and Mas de l´Alonso–el Pi Gros (Vilanova i La Geltrú). The charophyte assemblages comprise ten different species distributed among three distinctive aquatic environments, and are approximately simultaneous to major fossil vertebrate sites of these basins. *Sphaerochara ulmensis*, *Chara* cf. *vulgaris*, *Chara molassica* var. *notata*,

Lychnothamnus barbatus var. *antiquus*, *Lychnothamnus* sp., *Nitellopsis* (*Tectochara*) *merianii*, and *Nitellopsis* sp. occur associated to abraded benthic foraminifera in organic-rich claystones related to palustrine and shallow freshwater coastal lakes. *Lamprothamnium papulosum* forms monospecific assemblages in gypsum-claystone alternations attributed to a coastal brackish water salina. *Chara* cf. *hispida* and *Chara* sp. are found associated with ostracods in marls and limestones related to a permanent oligohaline and alkaline lake. The discovery of this aquatic flora sheds new light on the palaeoenvironmental conditions that prevailed in the Vallès–Penedès Basin during the Langhian in the context of the Mid-Miocene Climatic Optimum and in the Vilanova Basin during the Serravalian.

Keywords: Charophyta; Neogene; Aragonian; palaeolimnology; paleolake; palaeoecology

Introduction

In this work we describe three Miocene charophyte assemblages from the Vallès-Penedès and Vilanova i la Geltrú basins (Catalonia), which are near the northeastern coast of Spain.

The Vallès–Penedès Basin is one of the best known Miocene basins of eastern Iberia, mostly famous by its dense and continuous land mammal record that comprises hundreds of localities and thousands of specimens (see Casanovas-Vilar et al. 2016a and references therein). A relatively rich fossil pollen and leaf flora has also been documented from this basin (Bessedik 1985; Sanz de Siria Catalán 1993, 1994, respectively), allowing for a comparison with other Southern European floras. Despite its rich continental record, quite surprisingly fossil charophytes have yet to be reported from this area.

In the Iberian Peninsula Miocene charophytes have been described in detail from several basins, including the Ebro Basin (e.g., Feist et al. 1994), the Loranca Basin (e.g., Julià de

55 Agar 1991), the Teruel Basin in the Iberian Chain (e.g., Ludwig 1987) and the Portuguese
56 part of the Tagus Basin (Soulié-Märsche 1978). Less remarkable records include the
57 Intermediary Depression in Central Spain (Ortíz et al. 1998), La Cerdanya Basin in the
58 Eastern Pyrenees (e.g., Soulié-Märsche and Martín-Closas 2003) and from the Balearic
59 Islands (Martín-Closas and Ramos 2005). The state of the art about Iberian Miocene
60 charophytes surprisingly contrasts with the lack of charophytes studies from the Vallès–
61 Penedès Basin, and more considering that both land vertebrates and marine mollusks have
62 been thoroughly studied since the late 19th Century.

63 In this work we describe the first fossil charophyte assemblages from the Vallès–Penedès
64 Basin and use them to provide accurate palaeoenvironmental reconstructions of Miocene
65 continental aquatic environments. These derive from three distinct localities, els Casots
66 and Vilobí del Penedès, located in the southern sector (Penedès) of the Basin, and Mas
67 de l´Alonso–el Pi Gros, located in the western sector of the Vilanova i La Geltrú sub-
68 basin (Fig. 1). The els Casots and Vilobí del Penedès localities have been accurately dated
69 by means of bio- and magnetostratigraphy to about 16 Ma (see following section), that is
70 coinciding with the onset of the Miocene Climatic Optimum (MCO). The MCO
71 represented a brief greenhouse interval between ~17 and 15 Ma characterized by an
72 interruption of the Antartic icesheet build up (Zachos et al. 2001, 2008; Foster et al. 2012)
73 and mid-latitude temperatures as much as 3 ºC (You et al. 2009) or even 7 ºC
74 (Steinthorsdottir et al. 2020) higher than present. Fossil charophytes from both localities
75 (els Casots and Vilobí del Penedès) not only represent the first charophyte assemblages
76 from the Vallès-Penedès, but also provide new palaeoenvironmental information on
77 continental aquatic environments during the MCO in the western Mediterranean. The
78 sites from the Vilanova Basin i.e. Mas de l'Alonso and el Pi Gros date back to the

Serravallian (see below), that is, they postdate the MCO and coincides with a time of gradual cooling (see Zachos et al., 2001, 2008; Steinthorsdottir et al., 2020).

The three outcrops studied, els Casots, Vilobí del Penedès and Mas de l'Alonso–el Pi Gros correspond to three different palaeoenvironments, ranging from the late Burdigalian to the Serravalian. They record a diverse charophyte flora and show the potential interest that the study of fossil charophytes has for the understanding of the Vallès–Penedès non-marine palaeoenvironments. The presence of other microfossils (foraminifers and ostracods) provide further information on the palaeoenvironments associated to the charophyte flora.

Geological setting

The Vallés–Penedès Basin is part of a large system of Neogene grabens that mark the present eastern Iberian coastline, continuing further offshore (Roca and Guimerà 1992; Roca et al. 1999; Cabrera et al. 2004). These basins are part of the so-called València Trough which originated because of the opening of the western Mediterranean during the late Oligocene and Miocene (Roca et al. 1999; Roca 2001).

The Vallès–Penedès Basin is bounded by NE-SW oriented normal faults that formed after the tectonic inversion of ancient alpine compressional structures during the late Oligocene to Early Miocene (Fontboté 1954; Roca and Guimerà 1992). These limit the basin, which is 100 km long by 12-14 km wide, with the surrounding horsts of the Catalan Litoral Ranges. The Vallès-Penedès main fault is located in its northwestern margin, where the basement is attained at up to 4000 m depth (Bartrina et al. 1992; Roca et al. 1999). Basin basement, and corresponding sediment thickness, gently grades far away from the active margin towards the southeastern margin of the basin to just a few meters (Cabrera et al. 1991). The southwestern margin of the basin is only affected by minor faults which were overlapped by Early to Middle Miocene sedimentary sequences (Cabrera 1981a; Cabrera

and Calvet 1996). These were later fractured as result of minor fault reactivations (Cabrera 1981a; Cabrera and Calvet 1996). The basin is divided into two distinct sectors or sub-basins, Vallès and Penedès, by the NW-SE oriented Llobregat fault (Fontboté 1954; Cabrera and Calvet 1996). The semi-graben also shows a strong internal compartmentation due to the occurrence of small horsts and grabens, broadly parallel to the main fault (Permanyer 1990; Cabrera and Calvet 1996).

The Miocene record of the Vallès-Penedès basin has been subdivided into four main lithostratigraphic units which have been dated combining bio- and magnetostratigraphy (Agustí et al. 1985; Cabrera and Calvet 1996; Cabrera et al. 1991; Casanovas-Vilar et al. 2016b; de Gibert and Casanovas-Vilar 2011):

(1) Basal Breccia Unit. This consists of monogenic conglomerates and breccias and crops out only at a few points in the Garraf-Montnegre horst. It dates back to the Ramblian mammal age (early Burdigalian) in the Vallès sector and it is younger in the Penedès, dating back to the early Aragonian (late Burdigalian and earliest Langhian; de Gibert and Casanovas-Vilar 2011; Casanovas-Vilar et al. 2022).

(2) Lower Continental Units. Consist of alluvial fan red beds, including conglomerates, sandstones, and siltstones. Older alluvial fan deposits within this unit were sourced from the southeastern basin margin, while younger ones were also sourced from the northwestern reliefs and expanded in the lowlands covering wider areas. Shallow carbonate and evaporite lacustrine systems developed in zones of the southeastern part of the basin (Cabrera et al. 1979; Cabrera 1981a, b), such as the Subirats detritic-carbonatic system, which includes the site of els Casots (see Casanovas-Vilar et al. 2022). This unit mainly covers the Burdigalian (Early Miocene) and coincides with the rifting phase in the Vallès–Penedès Basin (Cabrera et al. 2004). The els Casots site has been dated to the earliest Langhian (15.9 Ma).

(3) The Marine and Transitional Units. These developed during the late Burdigalian to the early Serravallian and were related to a global sea-level rise that took place in the context of the MCO between 17 and 15 Ma (Miller et al. 2020). These also coincide with the beginning of the post-rift phase, when the faults that bounded the southeastern margin of the basin became inactive and were onlapped and overlapped by the sedimentary infill (Cabrera and Calvet 1996; Cabrera et al. 1991, 2004; Roca et al. 1999). At least three episodes of marine transgression and regression are recorded in the basin: late Burdigalian, Langhian and early Serravallian (Cabrera et al. 1991; Cabrera and Calvet 1996; Roca et al. 1999; de Gibert and Casanovas-Vilar 2011; Casanovas-Vilar et al. 2016b). Coastal saline lakes (sabkhas) developed just below the marine units in the area of Vilobí del Penedès, which represents a lifted block of the basin basement (Permanyer 1990). A diverse set of gypsum deposits up to 60 m thick developed in these sabkhas (Ortí and Pueyo 1976; Agustí et al. 1990). These gypsum deposits are overlain by claystones, which have yielded various charophyte assemblages, that are ultimately covered by oyster-rich greyish claystones and bioclastic limestones corresponding to the Langhian transgression. The gypsum units have been generally correlated to the late Burdigalian (Ortí and Pueyo 1976; Agustí et al. 1990; de Gibert and Casanovas-Vilar 2011), while the overlying claystones, which include small mammal fossils, indicate a younger, earliest Langhian, age (Jovells-Vaqué, 2020).

(3) Upper Continental Units. These cover the Serravalian and Tortonian and represent the late post-rift phase in the basin (Cabrera et al. 2004). They consist of alluvial fan deposits that were sourced from the reliefs in the northwestern margin while the Vallès-Penedès main fault remained active (Agustí et al. 1985, 1997; Cabrera and Calvet 1996; Roca et al. 1999; Casanovas-Vilar et al. 2016a, b; de Gibert and Casanovas-Vilar 2011). Most of the fossil vertebrate sites of the Vallès-Penedès Basin are located in the distal to marginal

facies of alluvial fan systems (Casanovas-Vilar et al. 2016 a, b), but this unit has not yielded charophyte localities thus far.

There are several smaller grabens next to the coast, south of the Garraf-Montnegre horst of the Catalan Coastal Ranges. These include the Pla de Barcelona, Baix Llobregat, Sant Andreu de la Barca, Olesa de Bonesvalls and Vilanova basins, and all formed in the context of the same extensional processes that originated the Vallès-Penedès Basin.

The Vilanova basin is about 5 km wide by 11 km long (Fig. 1). Same as the Vallès-Penedès, its northwestern margin is limited by a major normal fault affecting the pre-Miocene basement, while the southeastern margin is defined by minor normal faults that are overlapped by Quaternary sediments or are currently under sea in most of the basin (Ramos-Guerrero et al. 1996). Ramos-Guerrero et al. (1996) defined up to four litostratigraphic units attaining a maximum thickness of about 400 m. The oldest unit (M0) is represented by the marginal complex (breccias) associated and genetically related to the main faults that bound the basin. The other three units show a vertical evolution from continental alluvial environments at the base (M1), freshwater and brackishwater lacustrine facies (M2), to marine (littoral and restricted shelf-bay) at the top (M3). The charophyte assemblages studied here (localities of Mas de l'Alonso and el Pi Gros) have been recovered from the M2 unit (Intermediate Detrital-Carbonate Unit) which is mainly composed of lacustrine marls and limestones. These litostratigraphic units have been correlated to the Serravallian, although the lowermost alluvial conglomeratic units may correspond to Langhian (Cabrera et al. 2004).

----------Figure 1 near here----------

Materials and methods

178 The fossil flora herein studied has been recovered from soft rocks (claystones and marls)
179 from three distinct localities: els Casots, Vilobí del Penedès, in the Penedès sub-basin and
180 Mas de l´Alonso–el Pi Gros, in the Vilanova i la Geltrú sub-basin (Fig. 1). The
181 coordinates of these localities are: els Casots (Subirats), 41°24'56.57"N 01°48'41.78"E;
182 Vilobí del Penedès, 41°23'15.24"N, 01°39'10.90"E; Mas de l´Alonso (Vilanova i la
183 Geltrú), 41°14'57.28"N, 1°43'39.59"E, and el Pí Gros (Vilanova i la Geltrú),
184 41°14'52.57"N, 01°42'50.09"E.

185 In total, 12 samples of 2 kg each one were treated to extract the microfossils. Samples
186 were disaggregated in water, hydroxide peroxide and sodium carbonate and later wet-
187 sieved using sieves with mesh apertures of 1, 0.5, and 0.3 mm. In case of Vilobí del
188 Penedès (sample V6/7), about 2000 kg of sediments were screen-washed during a field
189 campaign undertaken by the Institut Català de Paleontologia (ICP) in the 1990s. The field
190 campaign focused on the recovery of microvertebrate remains and the smallest mesh
191 aperture used during the sieving process was 0.5 mm. In April 2021, 2 kg of sediments
192 were taken from the same outcrop to recover a smaller microfossil fraction (200 – 500
193 µm), which was lost in the previous campaign because a larger mesh size was used.

194 Nine out of the twelve studied samples yielded microfossils including gyrogonites,
195 ostracod carapaces, skeletons of foraminifera, and fish teeth (Fig. 2). Microfossils were
196 sorted after inspecting the residue washed sediment under a light microscope. Selected
197 gyrogonites were measured using the software Motic Images Plus 2.0 ML in a
198 stereomicroscope Motic BA310 with a built-in digital camera housed in the Departament
199 de Dinàmica de la Terra i de l´Oceà (Facultat de Ciències de la Terra), Universitat de
200 Barcelona). The biometric parameters considered were the gyrogonite height (µm), the
201 gyrogonite width (µm), the number of spiral turns observed in lateral view and the
202 isopolarity index (gyrogonite height/gyrogonite width × 100). Well-preserved

microfossils were selected and photographed using the scanning electronic microscope (SEM) QUANTA 200 located at the Centres Científics i Tecnològics, Universitat de Barcelona (CCiTUB). Thin-sections, ca. 30 μm in thickness, were prepared from four limestone beds from els Casots and Mas de l´Alonso-el Pi Gros localities (Fig. 2). The microfossils illustrated herein are curated at the Institut Català de Paleontologia Miquel Crusafont (ICP) at Sabadell (Catalonia, Spain) with catalogue numbers IPS122528, IPS122530 and IPS127514 to IPS127517.

Results

Depositional setting and age

Els Casots (Subirats)

Els Casots is a key vertebrate fossil site situated in the municipality of Subirats, in the south-western margin of the Penedès sub-basin (Fig. 1). The Miocene succession at els Casots area directly overlies the basement, which consists of Mesozoic (mainly Early Cretaceous) marine carbonates (Casanovas-Vilar et al. 2022). The Miocene succession was studied by means of geological core sampling and is described in detail in Casanovas-Vilar et al. (2022). The core records a basal breccia followed by a 25 m-thick, cyclically-arranged mudstone/limestone succession that at the bottom includes thin (mm to dm thick) sub-bituminous coal deposits. The upper part of the cycle is a carbonate term that includes a variety of bioclastic- to micrite-dominated limestones that range from a few centimetres to a maximum of a couple of meters thick. The carbonate facies include bioclastic laminae alternated with very thin tufa-like carbonates (Cabrera 1979). Thin ferruginous laminae are associated to some of the bioclastic facies. Both carbonates and siliciclastic mudstones may include abundant plant fragments and freshwater gastropod shells or casts. The stratigraphic succession indicates lacustrine to palustrine environments with cyclically oscillating water level. This lacustrine/marshy succession

has yielded abundant and remarkably complete terrestrial vertebrate fossils in the excavated area of the site. The vertebrate fauna comprises up to 75 different vertebrate species including amphibians, reptiles, birds and mostly mammals. The finding of several articulated partial skeletons indicate that the site records an autochthonous to parautochthonous vertebrate assemblage (Casanovas-Vilar et al. 2022). The charophyte flora studied here was recovered from a 3.5 m thick section laterally equivalent to the vertebrate-bearing lacustrine/marshy layers (samples C1-C4 in Fig. 2). This consists of organic-rich claystones alternated with marls and a limestone bed (Figs 2 and 3A–B). Claystone beds range from 10 to 50 cm thick and show strong color variation from yellowish, gray to dark gray (Figs 2 and 3A–B). Some organic-rich claystones have yielded abundant plant remains such as leaf fragments of helophytic plants, e.g., *Typha*, well-preserved charophyte gyrogonites, abraded benthic foraminifera, plus vertebrate bones, sometimes in anatomical connection. Some claystone intervals present root marks. In some horizons abundant and irregular carbonate nodules occur (Fig. 3A). A 20 cm thick limestone bed with packstone texture includes mollusk shell fragments, 150 μm thin carbonate planar crusts (Fig. 3C-H) and oncoids (Fig. 3G), both interpreted as of cyanobacterial origin.

Claystones at els Casots are attributed to deposition in a quiet and shallow lake. The presence of nodular carbonates, mottling and root marks suggests that the original lacustrine sediments were subject to fluctuations of the water table leading eventually to subaerial exposure with a development of pedogenetic features, similar to those described elesewhere by Alonso-Zarza and Wright (2010) and references herein. Limited oxygen levels and rapid burial at the lake margins favored the preservation of mammal remains and helophytic plant leaves found in darker claystone intervals. Charophytes from these claystones grew under shallow lake conditions, while abraded remains of foraminifera

253 were probably whased in from nearby marine settings. The limestone layer studied at els
254 Casots is interpreted as deposited in a shallow pond. The occurrence of oncoids and
255 abundant mollusk-shell fragments suggest that higher hydrodynamic conditions and
256 perhaps trampling prevailed during its deposition. Moreover, the abundance of
257 cyanobacterial crusts and absence of charophyte remains in the same limestone bed
258 suggest that the water was eutrophic (Martín-Closas, 1999).

259 The lacustrine succession at els Casots ends rather abruptly and is followed by
260 reddish and mottled mudstones and sandstones that record subaerial distal channelized
261 alluvial fan facies. The continental deposits are in turn overlain by an oyster coquina and
262 a bioclastic quartzarenite, which marks the early Langhian transgressive surface in this
263 sector of the Vallès-Penedès Basin.

264 The age of els Casots is well constrained thanks to bio- and magnetostratigraphic
265 data (see Casanovas-Vilar et al. 2022). For a long time, this site was correlated to the
266 latest Early Miocene European mammal Neogene zone MN4, but the recent data indicate
267 a correlation to Aragonian subzone Cb, which corresponds to the earliest MN5.
268 Magnetostratigraphic data from the 30-m-thick els Casots succession indicate reverse
269 polarity which, coupled with the correlation to Aragonian subzone Cb (16.15–15.94 Ma;
270 boundaries after Van der Meulen et al. 2012), results in an estimated age of ~15.9 Ma for
271 the site of els Casots. Therefore, els Casots would coincides with the onset of the Miocene
272 Climatic Optimum (Zachos et al. 2001, 2008; Holbourn et al. 2015). Overall,
273 sedimentological, palaeobotanical (scarce macroflora remains) and faunal data indicate
274 that els Casots corresponds to an ancient freshwater lacustrine or palustrine environment
275 that developed in a tropical-subtropical climate with rainfall seasonality (Casanovas-Vilar
276 et al. 2022).

277

----------Figure 2 near here----------

----------Figure 3 near here----------

----------Figure 4 near here----------

Vilobí del Penedès

The section studied at Vilobí del Penedès overlies unconformably the Cretaceous limestone substrate (Fig. 1). The base of the sequence is represented by non-marine breccias, detritic red beds and limestones of the Lower Continental System, which in turn are overlain by a 60 m thick evaporitic sequence mainly composed of secondary gypsum but showing primary gypsarenite at the top (Ortí and Pueyo 1976; Ortí 1990). The succession follows with a 7-m-thick interval dominated by reddish and grey claystones which have yielded the charophyte flora studied herein (samples V1-V6/7 in Fig. 2.2) and micromammal remains that had been previously attributed to the early Aragonian, MN4 zone, corresponding to the latest Early Miocene (Agustí et al. 1985, 1990; Casanovas-Vilar et al. 2016a). However, the rodent fauna includes the same cricetid species recorded at els Casots (Jovells-Vaqué and Casanovas-Vilar 2021) and amongst the eomyids only the species *Ligerimys ellipticus* is present (Jovells-Vaquè 2020). Consequently, this favors a correlation with Aragonian subzone Cb and indicate an early Middle Miocene age (MN5) for the site instead (Jovells-Vaqué 2020). Therefore, it would be chronologically very close to other sites of the Vallès-Penedès Basin immediately before

301 the Langhian regional marine transgression, such as els Casots or Sant Mamet (Sant Cugat
302 del Vallès).

303 The upper part of the Vilobí del Penedès succession, which has been studied here in more
304 detail, can be subdivided into three intervals. The first one is 2.5 m thick and overlies a
305 laminated gypsarenite (Fig. 4A). It is composed of an alternation of primary gypsum and
306 greenish claystones rich in charophytes and ostracods. Up to 4 parasequences of gypsum-
307 claystone alternations can be distinguished (Fig. 4B). A semi covered greenish claystone
308 bed, 1.5 m thick, lays over the gypsum-claystone alternation and yielded a second,
309 species-rich charophyte assemblage (Fig. 4C). The second interval is represented by 2.5
310 m of reddish claystone covered by an oyster bank that marks the base of the third interval
311 (Fig. 4D), which is dominated by grey marls and bioclastic limestones rich in marine
312 fossils such as echinoderms and coralline rhodophytes.

313 The evaporitic succession at Vilobí del Penedès has been interpreted by Bitzer (2004) and
314 references therein as having been deposited in a restricted coastal lake or salina (sabkha).
315 The facies alternation of gypsum and claystone horizons with charophytes observed
316 above the evaporitic unit, suggests that sediments settled under fluctuating salinity
317 conditions within the coastal salina. Gypsum layers precipitated in hypersaline
318 conditions, of up to 110‰ according to Bitzer (2004), while claystone layers were
319 deposited in more diluted conditions, corresponding to brackish water, as shown herein.
320 Each gypsum-claystone parasequence can be interpreted as small transgressive-regressive
321 cycle within the salina (Fig. 2). The absence of evaporites and the presence of a diverse
322 charophyte assemblage in the overlying grey claystone beds indicate that diluted
323 conditions finally prevailed, corresponding probably to a coastal freshwater lake (Fig.
324 4C). Finally, the oyster bank and the bioclastic limestone located atop of the section marks
325 the onset of the Langhian regional marine transgression (Fig. 4D).

Mas de l´Alonso–el Pi Gros (Vilanova i la Geltrú):

The studied succession is located at the western margin of the Vilanova i la Geltrú basin (Fig. 1) and corresponds to the Intermediate Detrital-Carbonate Unit (M2) of Ramos-Guerrero et al. (1996). The outcrop at Mas de l´Alonso consists of dark grey organic-rich claystones with charophytes topped by a metric yellowish lacustrine limestone bed (Fig. 2.4). Two samples provided charophytes (samples MA1 and MA2 in Fig. 2.4). About 1 km westwards, at the el Pi Gros locality, a lateral equivalent of the same non-marine sequence crops out and shows a 3.5 m succession of yellowish limestone alternated with marls, claystones, and siltstones (Figs 2.3 and 5). Four horizons yielded charophytes, i.e., samples PG1-PG4 in Fig. 2.3. Light grey to yellowish limestone beds at the base of the el Pi Gros section range in thickness from 10 to 30 cm. They display wackstone-packstone textures and contain abundant microfossils such as ostracods and gyrogonites (Fig. 5C–H). These limestones are overlain by two parasequences of limestone beds with stromatolithic lamination covered by reddish bioturbated claystones (Figs 2.3 and 5B). The upper part of the section at el Pi Gros shows 0.5 m-thick cross-bedded calcarenite and is topped by a 0.6 m limestone bed displaying packstone textures rich in gyrogonites, charophyte thalli, dasycladaleans, ostracods, and potamidid gastropods (Fig. 2.3). Above these materials marine facies of the M3 Unit of Ramos-Guerrero et al. (1996) crop out. Despite some authors suggested that the M2 unit is Langhian in age (Batllori and Moreno 2003), the micromammals from fossil sites located within this unit indicate younger ages (Serravalian). The site of los Viñedos (Sant Pere de Ribes), yielded small vertebrate remains that are suscintly reported in Ramos-Guerrero et al. (1996). The revised faunal list includes the cricetids *Megacricetodon crusafonti* and *Hispanomys* cf. *decedens* which would indicate a correlation with the *Megarcricetodon crusafonti* + *Democricetodon larteti* Concurrent Range Subzone of the Vallès-Penedès Basin (Casanovas-Vilar et al.

2016b), thus indicating an age closer to 12.4–12.5 Ma, that is late Aragonian (chronologically equivalent to the late Serravallian). A second site, Sant Pere de Ribes 1, located at the Can Mestre quarry (Ramos-Guerrero et al. 1996), has yielded additional small mammal remains. These include just a few teeth that are assigned to *Democricetodon crusafonti* (referred to as *Renzimys bilobatus* in Ramos-Guerrero et al. 1996) a species that is first recorded during the late Aragonian in the Vallès-Penedès at 11.88 Ma (Casanovas-Vilar et al. 2016b) and slightly earlier (12.4 Ma) in the Calatayud-Montalbán Basin (Aragon; Van Dam et al. 2014). Therefore, unit M3 would belong to the late Serravallian as well.

According to Ramos-Guerrero et al. (1996), the sequence integrating the M2 and M3 units grades upwards from lacustrine to brackish and finally marine environments. The lacustrine conditions of Unit M2 were inferred because of the presence of freshwater gastropods, helophytic plant stems, and charophyte remains (Batllori and Moreno 2003 and references therein). The locality of el Pi Gros is well known by the diverse and rich mollusk fauna preserved as molds, and the bioerosion ichnofossils, both found in the overlying marine M3 Unit (Batllori and Moreno 2003; Belaústegui et al. 2018). In contrast, the fossils of the M2 Unit are poorly known.

Microfossils recovered from the lower marls at Mas de l'Alonso (sample MA-1, Fig. 3 and Table 1) and el Pi Gros (sample PG-2, Fig. 3, Table 1) are well preserved and do not show signs of fragmentation or abrasion. Moreover, ostracod carapaces frequently appear with the two valves articulated suggesting that they were buried *in situ*. The absence of charophyte thalli in these marls suggest that there was a certain selection of the original plant remains, and that gyrogonites may have been laterally transported from the shallower areas of the lake where they grew. The occurrence of rare and abraded foraminifera at Mas de l'Alonso is interpreted as result of transport from a nearby marine

coastal area. Altogether these data suggest that the depositional environment of these marls corresponded to a relatively deeper part of a freshwater lake. The overlying charophyte-rich limestones were deposited in shallower freshwater environments, where lime-producing organisms thrived. Wackestone–packstone textures suggest the prevalence of sublittoral lacustrine conditions (e.g., Gierlowski-Kordesch 2010). Higher in the series, the substitution of charophyte-rich marl and limestones by stromatolite limestones and reddish claystone suggest that palaeoenvironmental conditions changed, difficulting the growth of charophytes. The occurrence of the terrigenous red claystone atop of the stromatolite, probably indicating deposition in a floodplain, suggest that the nutrient input to the lake may have increased during the development of stromatolites, hindering the development of charophytes.

----------Figure 5 near here----------

Systematic palaeobotany (Charophytes)

Division Charophyta Migula, 1897

Class Charophyceae Smith, 1938

Order Charales Lindley, 1836

Family Characeae Richard ex C. Agardh, 1824

Subfamily Nitelloideae A. Braun in Migula, 1897

Genus *Sphaerochara* (Mädler, 1952) emend. Soulié-Märsche, 1989

Sphaerochara ulmensis (Straub, 1952) comb. nov. Grambast, 1962

Fig. 6A–I

1952. *Chara ulmensis* Straub, p. 470, pl. A, fig. 19.

1962. *Sphaerochara ulmensis* Grambast, p. 77.

Material: This species occurs at Vilobí del Penedès and Mas de l´Alonso–el Pi Gros (Table 1). Twenty-three gyrogonites were measured in sample MA1 and nine specimens in sample V6/7 (Table 2 in supplementary data).

Description: Gyrogonites from MA1 are small, 398–477 µm high (mean 437 µm) and 330–431 µm wide (mean 391 µm), prolate spheroidal in shape, with an isopolarity index of 112 (mean). Nine to ten spiral turns are visible in lateral view. Spiral cells are 53 µm high in average and ornamented with an irregular mid-cellular crest (Fig. 6F–H). The thickness of the mid-cellular crest can vary significantly, and it can stretch the complete width of the spiral cell (Fig. 6B, C and C–E). The apex is rounded in lateral view. The apical end of each spiral cell is ornamented with a small, individualized coma-shaped nodule (Fig. 6A). The basal plate is visible from the outside and it is located within a large pentagonal basal pore of ~75 µm across (Fig. 6D and I). The external part of the basal plate bears a central nodule (Fig. 6D and I). Gyrogonites from the sample V6/7 at Vilobí del Penedés (Fig. 6A–D) are ~175 µm larger and wider than specimens extracted from Mas de l´Alonso.

Remarks: This species shows strong morphological similarities to other ornamented *Sphaerochara* gyrogonites from the European Paleogene displaying mid-cellular crests such as *S. hirmeri* (Rasky 1945) Mädler 1952 and *S. labellata* Feist and Ringeade 1977. Gyrogonites of *S. ulmensis* are longer and show a higher ISI index than the two aforementioned taxa. Moreover, this species displays a thicker and more prominent mid-cellular crest. The subtle differences between these three coeval ornamented *Sphaerochara* species suggest that a comprehensive taxonomic revision should be conducted in future studies.

Fossil record and distribution: This taxon has been reported in several Paleogene and Neogene basins worldwide i.e., Europe, Middle East, and China mainly in sedimentary sequences ranging in age from the upper Rupelian (early Oligocene) to the Tortonian (Late Miocene). In Europe it is reported from several basins such as the Rhine Graben in North and Central Germany (Straub 1952; Schwarz 1997 and references therein); the Alpine Molasse in South Germany (Mädler 1955; Horn af Rantzien,1959; Reichenbacher and Schwarz 1997); the Provence (Feist-Castel 1977), and the Languedoc, both in France (Chellaï et al. 1982); the Ebro Basin in Catalonia (Feist et al. 1994); and the Cluj Basin in Romania (Baciu and Feist 1999). *S. ulmensis* has also been reported by Mädler and Staesche (1979) from several basins of Central Anatolia (Turkey), and Knobloch (1979) further recovered *S. ulmensis* in Neogene rocks from Iraq. In China, *S. ulmensis* is found in Oligocene deposits from the Bohai coastal region (Xinlun 1978) as well as in several Chinese provinces, such as Sichuan (Huang et al. 1988), Yunnan (Liu 1989), Xinjiang (Lu and Luo 1990) and Qinghai (Tang and Di 1991).

Palaeoecology: S. ulmensis is found in limestones attributed to well-developed lacustrine systems, e.g., the Trévaresse limestone Formation in Aix-en-Provence, France (Feist-Castel 1977). Based on the associated microfossils, Reichenbacher and Schwarz (1997) concluded that *S. ulmensis* was a halophobous taxon, adapted exclusively to freshwater habitats.

Subfamily Charoideae A. Braun in Migula 1897

Genus *Chara* Linnæus, 1753

Chara cf. *vulgaris* Linnæus, 1753

Fig. 6 J–N

1753. *Chara vulgaris* Linnæus, p. 1156

1989. *Chara vulgaris* var. *vulgaris* Soulié-Märsche, p. 97, pl. 22

Material: This taxon dominates the flora in the sample C4 from els Casots (Table 1). Fifty gyrogonites were measured (Table 2 in supplementary data).

Description: Gyrogonites are of medium size, 378–584 μm high (mean 466 μm) and 256–430 μm wide (mean 352 μm), showing a prolate to perprolate shape and an isopolarity index ranging between 112 and 166 (mean 133). Ten to thirteen (mainly eleven) convolutions are visible in lateral view (Fig. 6K–M). Spiral cells are flat to concave, non-ornamented and ~44 μm in height. Spiral cells expand at the apical area (Fig. 6J) forming a psilocharoid apex type (Feist et al. 2005). The base is rounded or slightly pointed showing a small pentagonal basal pore of ~48 μm in diameter (Fig. 6N).

Remarks: The population described herein is remarkably similar to gyrogonites of living *C. vulgaris* in morphlogical characters such as the apical and basal structure, gyrogonite width and convolution number in lateral view (Soulié-Märsché 1989; Sanjuan et al. 2017). However, the studied fossil sample shows gyrogonite heights ~100–150 μm shorter than living populations.

Fossil record and distribution: Fossils of *C. vulgaris* are poorly known in Neogene sedimentary sequences. Ghetti et al. (2002) reported gyrogonites of *C. vulgaris* from Late Miocene (early Messinian) rocks of the Velona Basin (Siena, Central Italy). Bathia et al. (1998) found this species in the Plio-Pleistocene intermountainous Himalayan basins (Kashmir, India). Fan et al. (1996) also recovered gyrogonites attributed to this taxon in upper Pleistocene lacustrine facies in the Bangong Co Basin (Western Tibet). Large samples of *C. vulgaris* were recovered by Soulié-Märsche (1991) and Soulié-Märsche et al. (2010) from Pleistocene/Holocene paleolakes from Chad, Algeria and Sudan (Africa).

Palaeoecology: Chara vulgaris thrives in many kinds of shallow non-marine waterbodies worldwide (Corillion 1972). This taxon grows in temporary ponds or permanent lakes from the depth of several centimeters to up to 1 m (Krause 1997). It can live in freshwater to oligohaline conditions, but calcified gyrogonites are only formed at salinities below 5 ‰ and in alkaline water (Ghetti et al. 2002 and references therein). It has also a wide tolerance to different trophic conditions including eutrophic water (Korsch 2016).

Chara molassica var. *notata* (Straub, 1952) comb. nov. Soulié-Märsche, 1989

Fig. 6O–U

1952. *Chara molassica* forma a Straub, p. 467, pl. A, fig. 4–5

1965. *Chara notata* Grambast and Paul, p. 245

1989. *Chara molassica* var. *notata* Soulié-Märsche, p. 146

Material: Fifty specimens were extracted from Vilobí del Penedès and fifteen gyrogonites from els Casots (Table 1). Thirty-five specimens were measured from the sample V6/7 (Table 2 in supplementary data).

Description: Gyrogonites are of medium size, 498–599 μm high (mean 520 μm) and 320–416 μm wide (mean 377 μm). They are subprolate in shape and display a wide isopolarity index value, ranging between 108 and 161 (mean 138). Eight to twelve (commonly ten) convolutions are visible in lateral view. Mean high of spiral cells is ~59 μm and they are concave and ornamented with isolated small tubercles regularly arranged in row (Fig. 6I, Q and T). Gyrogonites display a prominent psilocharoid-type apex (Fig. 6O and S). The apex is ornamented with enlarged apical tubercles (Fig. 6S). The base is rounded or slightly pointed showing a shallow pentagonal basal pore of ~36 μm in diameter (Fig. 6R and U).

Fossil record and distribution: Chara molassica var. *notata* has been recovered in latest Oligocene (Chattian) to Late Miocene (Tortonian) sedimentary sequences in Europe. Feist-Castel (1977) and Feist and Ringeade (1977) described populations of this taxon from the latest Oligocene/Early Miocene (Aquitanian) of the Provence and Aquitaine basins in France respectively. Large samples of *C. molassica* var. *notata* were later recovered in Aquitanian-aged rocks of the Alpine Molasse Basin in Switzerland (Berger 1983; Schwarz and Reichenbacher 1989). This variety is also well represented in the latest Oligocene/Early Miocene of the Rhine Graben, Germany (Schwarz 1997 and references therein). Julià de Agar (1991) reported this taxon from the Loranca Basin (Tagus Basin, Spain). In the Ebro Basin (NE Spain) *C. molassica* var. *notata* is well represented in Chattian to Tortonian non-marine deposits (Feist et al. 1994; González-Pardo 2012). This species was also reported from the Middle East by Knobloch (1979) who found it in the Miocene Fars Formation (Iraq).

Palaeoecology: Previous studies report this species in freshwater lacustrine facies (e.g., Feist and Ringeade 1977).

----------Figure 6 near here----------

Chara cf. *hispida* Linnæus, 1753

Fig. 7A–H

1753. *Chara hispida* Linnæus, p. 1156–1157

1989. *Chara hispida* var. *major* Soulié-Märsche, p. 92, pl. 23

1999. *Chara* cf. *hispida* var. *major* García, p. 311, Fig. 4a–e

518 *Material:* Hundreds of well-preserved gyrogonites have been recovered in the el Pi Gros
519 section (Table 1). One hundred specimens were measured from the sample PG2 (Table 2
520 in supplementary data).

521 *Description:* Gyrogonites are medium- to large-sized, ranging between 540–891 μm in
522 height (mean 726 μm) and 352–621 μm in width (mean 500 μm). The dominant
523 gyrogonite shape is prolate spheroidal to perprolate (Feist et al. 2005), with an isopolarity
524 index ranging between 106 and 206 (mean 145). Nine to twelve (commonly ten) spiral
525 cells are visible in lateral view (Fig. 7A–D). Spiral cells are flat to convex, about 88 μm
526 wide and without ornamentation. They become thinner towards the periphery of the apex.
527 The apex is psilocharoid and prominent, generally pointed (Fig. 7E–F). The base is also
528 pointed showing a small pentagonal basal pore of ~59 μm in diameter (Fig. 7G–H).

529 *Remarks:* The population at el Pi Gros displays smaller gyrogonites (~180 μm in length
530 and ~85 μm in width) than recent populations of *C. hispida* studied by Soulié-Marshé
531 (1989) or Détriché et al. (2009).

532 *Fossil record and distribution:* Fossils of *Chara hispida* have been described from
533 Quaternary sedimentary sequences of Europe, Africa and South America. Anadón et al.
534 (1987) reported gyrogonites of this species from the Pleistocene of the Guadix-Baza
535 Basin (SE Spain). Fossil samples are also reported from the Holocene lacustrine
536 sediments from the Wadi Shaw (Sudan) and intermountainous basins in the Middle Atlas
537 of Morocco (Soulié-Marsche 1991; Détriché et al. 2009). García (1999 and references
538 therein) reported gyrogonites of *C. hispida* from several Quaternary localities from
539 Argentina, i.e., Quebrada del Zonda (Province of San Juan), Laguna Salada Grande
540 (Buenos Aires Province), and Laguna del Bebedero (San Luis Province).

541 *Palaeoecology:* Extant *C. hispida* is a subcosmopolitan species thriving in lakes from
542 nearly all states in Europe, and a few localities in North Africa, the Caucasus, Central

543 Asia, and Eastern Siberia (Corillion 1972; Barinova et al. 2014 and references therein). It
544 dwells in alkaline permanent and well-oxygenated lakes at depths of up to 15 m.
545 However, this species mostly occurs between 0.5 and 7 m depth (Krause 1997). In spite
546 that preferred habitats of *C. hispida* are freshwater lakes, it can tolerate brackish water
547 (Mannschreck 2003). In agreement with habitat requirements of extant *C. hispida*, the
548 gyrogonite assemblage studied here would also be indicative of permanent and stable
549 freshwater lake conditions.

550 *Chara* sp.

551 Fig. 7I–M

552 *Material:* A few gyrogonites were found at el Pi Gros locality (Table 1). Three specimens
553 were measured in sample PG2 (Table 2 in supplementary data).

554 *Description:* Gyrogonites are very variable in size ranging between 612–825 μm in height
555 and 350–400 μm in width. The dominant gyrogonite shape is perprolate, with a very high
556 isopolarity index ranging between 161 and 206. Six to seven spiral cells are visible in
557 lateral view (Fig. 7J–L). Spiral cells are convex, without ornamentation. The apex is
558 psilocharoid and very prominent, generally pointed (Fig. 7I). The base is also pointed
559 showing a very small basal pore (Fig. 7M).

560 *Remarks:* This material could belong to extreme polymorphs of of *Chara hispida*, with
561 which it cooccurs in the same samples but in a lower proportion (Table 1). Stressful
562 environmental conditions are well known to result in the development of extreme
563 polymorphs in extant *Chara* species (e.g., Pukacz et al. 2012).

564 Genus *Lamprothamnium* J. Groves, 1916

565 *Lamprothamnium papulosum* (Wallroth, 1833) comb. nov. Groves, 1916

566 Fig. 7N–U

1833. *Chara papulosa* Wallroth, p. 107

1916. *Lamprothamnium papulosum* Groves, p. 336

1969. *Lamprothamnium priscum* Castel and Grambast, p. 940–941, pl. XXXII, figs 4–7

1989. *Lamprothamnium papulosum* Soulié-Märsche, p. 150–153, pl. XXXII

Material: Many gyrogonites were recovered from several samples at the base of the Vilobí del Penedès section (Table 1). Sixty specimens were measured from the sample V5 (Table 2 in supplementary data).

Description: Girogonites are of medium size, 569–711 μm high (mean 631 μm) and 348–542 μm wide (mean 469 μm), cylindrical or prolate in shape (Fig. 7N–Q), with an isopolarity index ranging from 113 to 177 (mean 135). Gyrogonites show a prominent apex of lamprothamnoid type (Fig. 7R–S), i.e., displaying a well-marked periapical depression (Feist et al. 2005). Seven to eleven (commonly 9) spiral cells are visible in lateral view. Spiral cells are concave, flat, or convex depending on the calcification degree and ~81 μm high. Gyrogonites are not ornamented. The base of the gyrogonite is rounded or slightly pointed with a small pentagonal pore, ranging in diameter from 40 to 60 μm (Fig. 7T–U).

Remarks: Fossil gyrogonites of *L. papulosum* from Vilobí del Penedés are ~75 μm widerand display a reduced number of spiral cells in lateral view than gyrogonites from the living populations of the same species from brackish waters of southern France studied by Soulié-Märsché (1989). The studied gyrogonites are morphologically closer to *Lamprothamnium priscum* Castel and Grambast, 1969, a fossil species synonymized with *L. papulosum* by Soulié-Märsche (1989).

590 *Fossil record and distribution:* Extant *Lamprothamnium papulosum* is a quasi-
591 cosmopolitan species distributed throughout the world except in North and Central
592 America (Corillion 1972; García and Chivas 2004). The oldest known *L. papulosum* was
593 reported by Castel and Grambast (1969) and referred to as *L. priscum*, from the early
594 Eocene deposits from the Corbières mountains (southern France) and further from the
595 early Eocene of Ksour Mountains in Algeria (Mennad et al. 2021). *Lamprothamnium*
596 *papulosum* has been found in several Quaternary deposits of North Africa (Soulié-
597 Märsche 1982, 1998, 2007).

598 *Palaeoecology: L. papulosum* is adapted to aquatic environments subject to salinity
599 fluctuations and can thrive in sub-saline to hyper-saline waters up to 68‰ in salinity
600 (Burne et al. 1980). Despite *Lamprothamnium* can live in hypersaline conditions, the
601 required salinity to produce oospores and gyrogonites should be 20–40‰ (Soulié-
602 Märsche 1998 and references therein). However, short periods of salinity close to 10‰
603 are also tolerated for germination of oospores and gyrogonites (Dubois, 1968).

604

605

606 ----------Figure 7 near here----------

607

608 Genus *Lychnothamnus* (Ruprecht, 1845) von Leonhardi, 1863 emend. A. Braun *in*
609 Braun et Nordstedt, 1882

610 *Lychnothamnus barbatus* (Meyen, 1827) comb. nov. von Leonhardi, 1863

611 *Lychnothamnus barbatus* var. *antiquus* Soulié-Märsche, 1989

612 Fig. 8A–C

1827. *Chara barbata* Meyen, p. 75, pl. e, figs 7 and 8.

1863. *Lychnothamnus barbatus* Leonhardi, p. 72.

1989. *Lychnothamnus barbatus* var. *antiquus* Soulié-Märsche, p. 155, pl. 37, figs 1–6.

Material: A few specimens were recovered from the sample V6/7 at Vilobí del Penedès (Table 1). Three gyrogonites were measured (Table 2 in supplementary data).

Description: Gyrogonites are large (878 μm high and 733 μm wide), ellipsoidal in shape with an isopolarity index of 120. In the few gyrogonites recovered, spiral cells do not display any modification in the width or thickness at the periphery of the apex (Fig. 8A). The apex is flat, and the base is tapered showing a small basal pore. Nine or ten concave spiral cells in lateral view separated by bicarinate sutures can be clearly observed near the base (Fig. 8B). They are 120 μm high and devoid of ornamentation.

Fossil record and distribution: Lychnothamnus barbatus var. *antiquus* has been found in several Miocene/Pliocene peri-Mediterranean lacustrine basins from Europe, North Africa, and the Middle East. It has been reported from the Ebro and the Cerdanya basins (NE Spain), Rio Maior (Portugal), Provence (France), Maoče (Montenegro), Çankırı (Turkey) and Bekaa in Lebanon (Sanjuan and Alqudah 2018 and references therein).

Palaeoecology: The living species *L. barbatus* mainly thrives in permanent lakes of northern Europe (Corillion 1972) where it forms dense meadows at depths ranging between 2 and 8 m. These extant populations grow in cold and oligo-mesotrophic waters of freshwater lakes, frequently associated to phreatic sources (Krause 1997; Brzozowski et al. 2019).

Lychnothamnus sp.

Fig. 8D–F

636 *Material:* Only one complete specimen has been found. This gyrogonite and other
637 fragments attributed to this taxon were recovered from sample MA1 at Mas de l´Alonso
638 (Table 1 and Table 2 in supplementary data).

639 *Description:* Gyrogonites are large, 1022 µm high and 777 µm wide, cylindrical in shape
640 with an isopolarity index of 131. Spiral cells are ornamented with a characteristic
641 midcelular crest (Fig. 8E). Spiral cells do not show any modification at the periphery of
642 the apex and show a constant width. The apex is flat and ornamented with coma-shaped
643 tubercles (Fig. 8D). The base is tapered showing a star-shaped basal funnel (Fig. 8F).
644 Eight concave spiral cells are visible laterally, being separated by bicarinate sutures. This
645 character can be clearly observed near the base.

646 *Remarks:* The small number of recovered specimens hinders their identification to the
647 species level, but the ornamentation of this gyrogonite suggests affinities with species
648 formerly attributed to the fossil genus *Stephanochara* Grambast, which was synonymized
649 with *Lychnothamnus* by Soulié-Märsche (1989).

650 Genus *Nitellopsis* Hy, 1889

651 Subgenus *Tectochara* Grambast and Grambast-Fessard, 1954

652 *Nitellopsis* (*Tectochara*) *merianii* (Al. Braun ex Unger, 1852) comb. nov. Grambast and
653 Soulié-Märsche, 1972

654 Fig. 8G–N

655 1852. *Chara merianii* Unger, p. 82, pl. 25, figs 10–12.

656 1954. *Tectochara merianii* Grambast et Grambast-Fessard, p. 668.

657 1972. *Nitellopsis* (*Tectochara*) *merianii* Grambast et Soulié-Märsche, p. 11.

Material: Fifty gyrogonites were recovered from sample V6/7 at Vilobí del Penedès and few fragments attributed to this taxon were found in sample MA1 (Table 1). Thirty-five specimens were measured (Table 2 in supplementary data).

Description: Gyrogonites are large, ovoidal (Fig. 8K–N), 781–1120 μm high (mean 958 μm) and 656–957 m wide (mean 824 μm), with an isopolarity index ranging between 104 and 135 (mean 116). Spiral cells are flat to convex. Seven to nine (frequently eight) spiral cells are visible in lateral view (116 μm high). Gyrogonites display a nitellopsidoid apex (Fig. 8G–H), i.e., spiral cells become thinner and narrower at the periapical zone (Horn af Rantzien 1959). The apex is flat and ornamented with large apical nodules. The basal pole is conical showing a basal pore within a wide pentagonal funnel, 292 μm in diameter (Fig. 8I–J), sometimes star-shaped (Fig. 8J).

Fossil record and distribution: This species has been widely reported from several Paleogene/Neogene basins from Europe, North Africa, the Middle East and Asia (Sanjuan and Alqudah 2018 and references therein). The oldest representatives of this species were discovered in latest Eocene (late Priabonian) deposits of the Ebro Basin (Sanjuan and Martín-Closas 2014). Later, this species expanded its biogeographic range following 4 distributional phases to become finally subcosmopolitan in the Northern Hemisphere during the Miocene (Soulié-Märsche et al. 1997; Soulié- Märsche et al. 2002; Sanjuan and Martín-Closas 2015).

Palaeoecology: Nitellopsis (*T*) *merianii* is considered the ancestor of the living species *Nitellopsis obtusa* (Sanjuan and Martín-Closas 2015). This taxon thrives in permanent, cold, and deep alkaline lakes at a depth range between 4–12 m, in large lakes of northern Europe, Asia and North America (Corillion 1972). This species cannot tolerate salinities higher than 5‰ (Katsuhara and Tazawa 1986).

Nitellopsis sp.

683 Fig. 8O–Q

684 *Material:* A few abraded gyrogonites were recovered from sample V6/7, Vilobí del
685 Penedès. Only two specimens were measured (Table 2 in supplementary data).

686 *Description:* Gyrogonites are very large (1289 μm high and 1051 μm wide), ovoidal, with
687 an isopolarity index of 123. Spiral cells are flat and ornamented with a nodular mid-
688 cellular crest (Fig. 8P). Eight or nine spiral cells are visible in lateral view (155 μm high).
689 The apex is flat and of nitellopsidoid type (Horn af Rantzien 1959), ornamented with
690 small apical nodules (Fig. 8O). The basal pole is conical showing a small basal pore, 97
691 μm within a star-shaped funnel (Fig. 8Q).

692 *Remarks:* The main difference between this species and *N.* (*T*) *merianii* is the size and the
693 ornamentation. However, the small number of recovered specimens hinders their
694 identification to the species level.

695

696 ----------Figure 8 near here----------

697

698 **Discussion**

699 ***Charophyte taphonomy and palaeoecology***

700 The non-marine deposits from els Casots, Vilobí del Penedés, and Mas de l´Alonso–el Pi
701 Gros studied in this work have yielded a diverse number of charophyte and two ostracode
702 species which have characteristic palaeoenvironmental distributions. Several of them
703 have living representatives, which allow for more accurated palaeolimnological
704 inferences for the wetlands developed in the Vallès-Penedès and Vilanova i la Geltrú
705 basins during the Langhian and Serravalian.

We distinguish three different assemblages in the depositional environments studied:

Charophytes from shallow lakes: The microfossil assemblage associated to shallow lakes varies locally. Charophyte assemblages at els Casots are dominated by *Chara* cf. *vulgaris*. This living species has wide ecological tolerance and lives in brackish or freshwater environments (estuaries, rivers, springs, ponds and lakes). It mostly occurs at very shallow depths, from several centimeters up to 1 m and can live in eutrophic water (Krause 1997). This species can withstand oligohaline conditions and it only produces gyrogonites at salinities up to 5 ‰ (Ghetti et al. 2002). Associated taxa include *C. molassica* var. *notata* and abraded tests of *Ammonia* sp. rotaliid foraminifera. *C. molassica* var. *notata* is an extinct species related to freshwater lakes. The dominance of *C. vulgaris* suggests very shallow water and that water trophism may have been high in the paleolake of els Casots.

The flora in the upper part of the Vilobí del Penedès section (samples V5 and V6/7) corresponds to a shallow lake as well. In this case the charophyte assemblage is dominated by *C. molassica* var. *notata*. Other, less abundant, species include *Sphaerochara ulmensis*, *Nitellopsis* (*Tectochara*) *merianii*, and *Lychnothamnus barbatus* var. *antiquus*. A few poorly-preserved skeletons of rotaliid foraminifera (*Ammonia* sp.) also occur and are considered allochthonous to the lake. Charophytes indicate the prevalence of freshwater conditions. The occurrence of *Nitellopsis* (*Tectochara*) *merianii* and *Lychnothamnus barbatus* var. *antiquus* (ancestors of the extant species *Nitellopsis obtusa* and *Lychnothamnus barbatus*, respectively) thrive today in permanent, relatively deep (2–8m), oligotrophic lakes with salinities not exceeding 5‰. The ecological requirements of the charophyte assemblage at Vilobí del Penedès suggest that the lake was more stable and oligotrophic than the contemporary lake of els Casots.

731 Finally, the assemblage from Mas de l´Alonso (sample MA1) also corresponds to shallow
732 lacustrine conditions. In spite of the scarce material recovered the charophyte assemblage
733 is quite diverse and also includes rare *Ammonia* sp. foraminifera. The charophyte
734 assemblage is constituted by *Sphaerochara ulmensis*, *Chara* cf. *hispida*, *Lychnothamnus*
735 sp. and fragmented gyrogonites attributed to *Nitellopsis* (*Tectochara*) *merianii*. This
736 assemblage indicates the prevalence of shallow freshwater conditions. *Ammonia* sp. tests
737 show evident signs of abrasion and are considered allochthonous, being probably
738 transported from nearby marine settings.

739 *Charophytes from coastal salinas*: Assemblages from Vilobí del Penedès (lower part of
740 the section) are dominated by the charophyte species *Lamprothamnium papulosum*,
741 which occurs associated to abraded ostracod carapaces. *L. papulosum* is the most
742 halotolerant species among living charophytes, surviving at salinities up to 70‰ (Burne
743 et al. 1980). Despite withstanding such hypersaline conditions, living populations of *L.*
744 *papulosum* require salinities around 20‰ (maximum 40‰) to produce gyrogonites
745 (Soulié-Märsche 1998 and references therein). The presence of monospecific
746 assemblages of *L. papulosum* at Vilobí del Penedès indicates the prevalence of brackish
747 water conditions, limiting the development of other charophyte species (Fig. 10). Several
748 germinated gyrogonites indicate that seasonally the palaeosalinity could have been going
749 down to 10‰ for short periods of time.

750

751 ----------Figure 9 near here----------

752

753 *Charophytes from permanent lakes*: Based on the assemblages from el Pí Gros, two
754 charophyte species, *Chara* cf. *hispida* and *Chara* sp., and two ostracod taxa, *Heterocypris*

salina Brady 1868 (Fig. 9A–D) and a probable leptocytherid (Fig. 9E–J) are present. The presence of articulated valves suggests *in situ* burial. Gyrogonites of *Chara* cf. *hispida* are by far the dominant charophyte remains. Living meadows of *C. hispida* mainly grow in alkaline permanent freshwater lakes at a depth up to 15 m, mainly between 0.5 and 7 m (Krause 1997). This is an eurythermal species preferring calcareous and well-oxygenated waters (Barinova et al. 2014 and references therein), which can also tolerate brackish water conditions, as reported from the Baltic Sea (Mannschreck 2003).. *Chara hispida* shares similar habitat preferences with other *Chara* species and with *Nitellopsis obtusa* (Barinova et al. 2014). While charophyte thalli are absent in the marls, charophyte gyrogonites are very well preserved showing the endocalcine and ectocalcine layers intact, without traces of corrosion or dissolution, thus evidencing that they were buried *in situ* or near the production area. The ostracods found in these lacustrine facies provide significant information about the characteristics of the palaeo-waterbody at el Pi Gros. The leptocytherid species is similar to *Leptocythere* gr. *psammophila* in Gliozzi et al (2005). *Heterocypris salina* Brady, 1868 is widely distributed across Europe, West Asia, and North Africa inhabiting several types of waterbodies, from freshwater springs and wells to littoral zones of seas (Meisch, 2000; Gusakov et al. 2021). This species is found in slightly saline coastal and continental waters with salinities ranging from 5 to 35‰ (Gusakov et al. 2021), although Meisch (2000) reports that it is more usually associated with oligosaline waters, with an optimum salinity preference of around 6 ‰. Meisch (2000) further maintains that the species can also live in freshwater so that its presence should not be regarded as indicative of a saline waterbody in the absence of supporting evidence. Although Miocene leptocytherids have been reported from both marine brackish and athalassic saline environments (Gliozzi et al. 2005), the co-occurrence of the specimens with *H. salina*, together with additional micropalaeontological evidence,

780 suggests that el Pí Gros corresponds to lacustrine and oligohaline waterbody (Fig. 10).
781 This interpretation is consistent with the conclusions of Gliozzi et al (2005), who have
782 previously reported the co-occurrence of leptocytherids, including *Leptocythere* gr.
783 *psammophila* with *Heterocypris salina* from Seravallian lacustrine or palustrine
784 sediments from the Iberian Peninsula.

785

786 ----------Figure 10 near here----------

787

788 **Conclusions**

789 Middle Miocene (Langhian–Serravallian) lacustrine deposits of the Vallès–Penedès and
790 Vilanova i la Geltrú basins (SW of Barcelona) are here analyzed from the
791 sedimentological and palaeoenvironmental viewpoints. The three localities studied, i.e.,
792 els Casots (Subirats), Vilobí del Penedès, and Mas de l´Alonso–el Pi Gros (Vilanova i la
793 Geltrú), yielded a well-preserved charophyte assemblage compprising ten different
794 species. The recovered flora shows a characteristic palaeoenvironmental distribution and
795 sheds new light on the prevailing palaeolimnological characteristics of the wetlands in
796 the coastal basins of NE Iberia during the Middle Miocene. Facies analysis, taphonomy
797 and palaeoecology of the recovered taxa allows for the distinction of three different
798 palaeoenvironmental settings: shallow lake, coastal salina, and permanent stable lake.
799 Claystones related to shallow lakes occur in the three studied localities and have yielded
800 *Sphaerochara ulmensis*, *Chara* cf. *vulgaris*, *Chara molassica* var. *notata*,
801 *Lychnothamnus barbatus* var. *antiquus*, *Lychnothamnus* sp., *Nitellopsis (Tectochara)*
802 *merianii*, and *Nitellopsis* sp. This flora is unevenly distributed owing to local
803 palaeolimnological conditions. Mesotrophic to eutrophic conditions dominated the

804 Langhian palaeolake at els Casots, while more oligotrophic and stable conditions might
805 have prevailed at the upper part of the Vilobí del Penedès (Langhian) section and at Mas
806 de l'Alonso (Serravallian). The occurrence of abraded tests of benthic foraminifera
807 suggests that these freshwater lakes were situated close to the coastline. Facies related to
808 coastal salinas are only found at the base of the Vilobí del Penedès section (Langhian)
809 and are characterized by primary gypsum beds alternated with greenish claystones rich in
810 *Lamprothamnium papulosum*. Monospecific populations of this halotolerant taxon
811 indicate the prevalence of brackish waters with salinity fluctuations from low to
812 hypersaline concentrations. However salinities of around 20‰ are needed for the
813 production of gyrogonites. Finally, charophytes found in marls and limestones attributed
814 to permanent stable lakes occurs at el Pi Gros (Serravallian). The lake was inhabited by
815 *Chara* cf. *hispida* and *Chara* sp. as well as the ostracod species ?*Leptocythere* gr.
816 *psammophila* and *Heterocypris salina*, indicating the prevalence of oligohaline and well
817 oxygenated waters.

818 This is the first in-depth study of the charophytes from the Vallès-Penedès and Vilanova
819 basins. The results presented here show that charophytes are crucial for accurately
820 reconstructing palaeolimnological conditions, such as the water salinity, trophism or
821 depth. The combined study of charophytes and other microfossils, such as ostracods and
822 foraminifera, even improve such palaeoenvironmental inferences, especially regarding
823 salinity.

824 This study provides just a limited view of the total range of palaeoenvironments recorded
825 in this area. The whole Vallès sector and other associated sub-basins such as Sant Andreu
826 de la Barca, which contains mainly fluvio-lacustrine facies, have yet to be studied but
827 preliminary results indicate that they are also rich in charophyte fossils. Perhaps more
828 importantly, the combined continental record of these Catalan coastal basins covers

almost the entire Miocene, therefore allowing for the study of the evolution of terrestrial wetland ecosystems along protracted time intervals.

Acknowledgments

This study was funded by the project IBERINSULA (PID2020-113912GB-100 / AEI / 10.13039/501100011033) of the Spanish Research Agency (AEI) and the European Regional Development Fund (ERDF) and to project SGR2017-841 from the AGAUR Research Agency (Catalan Autonomous Government). We thank Dr. Carles Ferràndez (Department of Earth and Ocean Dynamics, Universitat de Barcelona) for his advice in the determination of benthic foraminifera. Alejandro Gallardo (Laboratory of Palaeontology, Department of Earth and Ocean Dynamics, Universitat de Barcelona) is acknowledged for preparing the thin sections. We are also very thankful to David Artiaga of the *Centres Científics i Tecnològics, Universitat de Barcelona* (CCiTUB) for his technical support during the SEM sessions. Josep Rovira (Vilobí del Penedès) is acknowledged for reporting us the charophyte beds from this locality. Dave Horne (Queen Mary, University of London) advised on the ostracod identification. We also thank the editor G. Dyke and the reviewer I. Soulié-Märsche for constructive comments during the peer-review process.

850 **References**

851 Agardh CA. 1824. Systema Algarum. Lund, Lundae Literis Berlingianis, 312 p.

852 Agustí J, Cabrera L, Moyà-Solà S. 1985. Sinopsis estratigráfica del Neógeno de la fosa
853 del Vallés-Penedés. Paleontologia i Evolució. 18:57–81.

854 Agustí J, Cabrera L, Domènech R, Martinell J, Moyà-Solà S, Ortí F, de Porta J. 1990.
855 Neogene of the Penedès area (Prelittoral Catalan Depression, NE Spain).
856 Paleontol Evol mem espec. 2:187–207.

857 Agusti J, Cabrera L, Garces M, Pares JM. 1997. The Vallesian mammal succession in
858 the Vallès-Penedès Basin (northeast Spain): Paleomagnetic calibration and
859 correlation with global events. Palaeogeogr. Palaeoclimatol. Palaeoecol. 133 (3-
860 4): 149–180.

861 Alonso-Zarza AM, Wright VP. 2010. Palustrine carbonates. In: Alonso-Zarza AM,
862 Tanner LH, editors. Carbonates in Continental Settings. Facies, Environments and
863 Processes: Developments in Sedimentology, 61. Elsevier: Amsterdam, p. 103–
864 126.

865 Anadón P, Julià R, De Deckker P, Rosso JC, Soulié-Märsche I. 1987. Contribución de la
866 paleolimnología del Pleistoceno inferior de la Cuenca de Baza (sector Orce-Vetna
867 Micena). Paleontol Evol. mem. espec. 1:35–72.

868 Baciu C, Feist M. 1999. Les charophytes Oligocènes du nord-ouest de la Transylvanie
869 (Roumanie). Acta Palaeontol. Roman. 2:27–29.

870 Barinova S, Romanov R, Solak CN. 2014. New record of *Chara hispida* (L.) Hartm.
871 (Streptophyta: Charophyceae, Charales) from the Işıklı Lake (Turkey) and Critical
872 Checklist of Turkish Charophytes. Nat Resour Conserv. 2 (3):33–42.

873 Bartrina MT, Cabrera L, Jurado MJ, Guimerà J, Roca E. 1992. Evolution of the central
874 Catalan margin of the Valencia trough (western Mediterranean). Tectonophysics.
875 203(1):219–247. https://doi.org/10.1016/0040-1951(92)90225-U

876 Bathia SB, Soulié-Märsche I, Gemayel P. 1998. Late Pliocene and Early Pleistocene
877 charophyte floras of the Haripur Formation, Kerawa Group, Kashmir, India. N.
878 Jb. Geol. Paläont. Abh. 210 (2):185–209.

879 Batllori J, Moreno J. 2003. Nota preliminar sobre la malacofauna (Gastropoda) del Miocè
880 del Pi Gros (Vilanova i La Geltrú, Garraf): Butll Inst Catalana Hist Nat. 71:117–
881 127.

882 Belaústegui Z, Domènech R, Martinell J. 2018. An ichnofossil-lagerstätte from the
883 Miocene Vilanova Basin (Ne Spain): Taphonomic and paleoecologic insights
884 related to bioerosion structures. Palaios 33:16–28.

885 Bessedik M. 1985. Reconstitution des environnements miocènes des régions nord-ouest
886 méditerranéennes à partir de la palynologie. PhD Thesis, Université des Sciences
887 et Techniques du Languedoc, Montpellier: 162 p.

888 Berger JP. 1983. Charophytes de 1'Aquitanien de Suisse occidentale. Essai de taxonomie
889 et biostratigraphie. Geobios 16 (1):5−37.

890 Bitzer K. 2004. Estimating paleogeographic, hydrological and climatic conditions in the
891 upper Burdigalian Vallès–Penedès Basin (Catalunya, Spain). Geol. Acta 2:321–
892 31.

893 Brady G. 1868. A monograph of the recent British Ostracoda. Transactions of the Linnean
894 Society of London 26:353–495.

895 Braun A, Nordstedt O. 1882. Fragmente einer Monographie der Characeen nach den
896 hinterlassenen Manusckripte A. Braun's, herausgegeben von Dr. O. Nordstedt.
897 Berlin, Abhandlungen der Kaiserlichen Akademie der Wisenschaften, p. 211.

898 Brzozowski M, Palomares-Cabanilles M, Kowalewski G, Pełechaty M. 2019.
899 Environmental factors responsible for the gyrogonite formation by an endangered
900 macroalga, *Lychnothamnus barbatus*, a fertility indicator of past and present
901 lacustrine ecosystems. Limnologica 77:125686.

902 Burne RV, Bauld JI, Deccker P. 1980. Saline lake charophytes and their geological
903 significance. J. Sediment. Petrol. 50:281–293.

904 Cabrera L. 1979. Estudio estratigráfico y sedimentológico de los depósitos continentales
905 basales de la depresión del Vallès-Penedès [dissertation]. Barcelona: Universitat
906 de Barcelona.

907 Cabrera L. 1981a. Influencia de la tectónica en la sedimentación continental de la
908 cuenca del Vallès-Penedès (provincia de Barcelona, España) durante el Mioceno
909 inferior. Acta Geol Hisp. 16:163–169.

910 Cabrera L. 1981b. Estratigrafía y características sedimentológicas generales de las
911 formaciones continentales del Mioceno inferior de la cuenca del Vallés Penedés
912 (Barcelona, España). Estud Geol. 37:35–44.

913 Cabrera L, Calvet F. 1996. The onshore Neogene record in NE Spain: Vallès-Penedès
914 and El Camp half-grabens (NW Mediterranean). In: Friend PF, Dabrio CJ,
915 editors. Tertiary Basins of Spain: Record of Crustal Kinematics. Cambridge,
916 United Kingdom: Cambridge University Press; p. 97–105.

917 Cabrera L, Calvet F, Guimerà J, Permanyer A. 1991. El registro sedimentario miocénico
918 en los semigrabens del Vallès–Penedès y de El Camp: organización secuencial y

relaciones tectónica-sedimentación. In: Colombo, F, editor. Libro Guía nº 4 del Congreso del GET, Vic: 132 p.

Cabrera L, Roca E, Garcés M, de Porta J. 2004. Estratigrafía y evolución tectonosedimentaria Oligocena superior-Neógena del sector central del margen Catalán (Cadena Costero-Catalana). In: Vera JA. editor. Geología de España, Sociedad Geológica de España, Instituto Geológico y Minero de España: 569–573.

Casanovas-Vilar I, DeMiguel D, Galindo J, Robles JM, Garcés M, Cabrera L. 2011. The continental Burdigalian (Early Miocene) of the Vallès–Penedès Basin (Catalonia, Spain). In: Pérez-García A, Gascó F, Gasulla JM, Escaso F. editors. Viajando a Mundos Pretéritos. Ayuntamiento de Morella, Morella: p. 93–100.

Casanovas-Vilar I, Madern A, Alba DM, Cabrera L, García-Paredes I, Van den Hoek Ostende LW, De Miguel D, Robles JM, Furió M, Van Dam J, Garcés M, Angelone C, Moyà-Solà S. 2016a. The Miocene mammal record of the Vallès–Penedès Basin (Catalonia). C R Palevol. 15:791–812.

Casanovas-Vilar I, Garcés M, Van Dam J, García-Paredes I, Robles JM, Alba DM. 2016b. An updated biostratigraphy for the late Aragonian and the Vallesian of the Vallès-Penedès Basin (Catalonia). Geol Acta 14 (3):195–217.

Casanovas-Vilar I, Garcés M, Marcuello A, Abella J, Madurell-Malapeira J, Jovells-Vaqué S, Cabrera Ll, Galindo J, Beamud E, Ledo JJ, Queralt P, Martí A, Sanjuan J, Martín-Closas C, Jiménez-Moreno G, Luján AH, Villa A, DeMiguel D, Sanchez I, Robles JM, Furió M, Van den Hoek Ostende LW, Sanchez-Marco A, Sanisidro O, Valenciano A, Garcia-Paredes I, Angelone C, Pons-Monjo G, Azanza B, Delfinor M, Bolet A, Grau-Camats M, Vizcaíno-Varo V, Mormeneo D, Kimura

943 Y, Moyà-Solà S, Alba DM. 2022. Els Casots (Subirats, Catalonia), a key site for
944 the Miocene vertebrate record of Southwestern Europe. Hist Biol. 34 (8):1494–
945 1508.

946 Castel M, Grambast L. 1969. Charophytes de l´Éocène des Corbières. Bull Soc Géol Fr.
947 7 (11):936–943.

948 Chellaï EH, Baudelot S, Crochet B, Feist M, Durand-Delga M. 1982. Preuves
949 paléontologiques de l´antériorité des Conglomérats de la Grésine (Éocène
950 supérieur) par rapport à la Molasse oligocène de l´Albigeois (Tarn). C. R. Acad.
951 Sci. Paris 295:683–690.

952 Corillion R. 1972. Les Charophycées de France et d'Europe Occidentale. Travaux du
953 Laboratoire de Botanique de la Faculté des Sciences d'Angers, Angers: 11–12,
954 499 p.

955 de Gibert JM, Casanovas-Vilar I. 2011. Contexto geológico del Mioceno de la cuenca del
956 Vallès-Penedès. Paleontologia i Evolució. Mem. espec. 6: 39–45.

957 Détriché S, Bréhéret JG, Soulié-Märsche I, Karrat L, Macaire JJ. 2009. Late Holocene
958 water level fluctuations of Lake Afourgagh (Middle-Atlas Mountains, Morocco)
959 inferred from charophyte remains. Palaeogeogr Palaeoclimatol Palaeoecol.
960 283:134–147.

961 Dubois, A. 1968. Observations sur la morphologie et la biologie des formes naines de
962 *Lamprothamnium papulosum* J. Groves (Characées). Naturalia Monspeliensia Ser
963 Bot. 19:37–41.

964 Fan H, Gasse F, Huc A, Li Y, Sifeddine A, Soulié-Märsche I. 1996. Holocene
965 environmental changes in Bangong Co basin (Western Tibet). Part 3: Biogenic
966 remains. Palaeogeogr Palaeoclimatol Palaeoecol. 120:65–78.

967 Feist-Castel M. 1977. Etude floristique et biostratigraphique des Charophytes dans les
968 series du Paleogene de Provence. Géol. Médit. 4:109–138.

969 Feist M, Ringeade M. 1977. Étude biostratigraphique et paléobotanique (charophytes)
970 des formations continentales d'Aquitaine, de l'Éocène supérieur au Miocène
971 inférieur. Bull Soc Géol Fr. 7:341–354.

972 Feist M, Anadón P, Cabrera L, Choi SJ, Colombo F, Saez M. 1994. Upper Eocene-
973 Lowermost Miocene charophyte in the Ebro Basin (Spain). Contribution to the
974 charophyte biozonation in Western Europe. Newsl Stratigr. 30:1–32.

975 Feist M, Grambast-Fessard N, Guerlesquin M, Karol K, Lu H, Mccourt RM, Wang Q,
976 Shenzen Z. 2005. Treatise on Invertebrate Paleontology. Part B., Protoctista 1.
977 Charophyta, The Geological Society of America, Kansas: 170 p.

978 Fontboté JM. 1954. Las relaciones tectónicas de la depresión del Vallès–Penedès con la
979 Cordillera Prelitoral Catalana y con la Depresión del Ebro. In: CSIC editor. Tomo
980 extraordinario de trabajos geológicos publicado con motivo del 80 aniversario del
981 nacimiento del profesor Eduardo Hernández-Pacheco. R Soc Esp Hist Nat. p. 281–
982 310.

983 Foster GL, Lear CH, Rae JWB. 2012. The evolution of pCO2, ice volume and climate
984 during the middle Miocene. Earth Planet Sci Lett. 341–344:243–254.
985 https://doi.org/10.1016/j.epsl.2012.06.007

986 García A. 1999. Quaternary charophytes from Salina del Bebedero, Argentina: Their
987 relation with extant taxa and palaeolimnological significance. J Paleolimnol.
988 21:307–323.

989 García A, Chivas AR. 2004. Quaternary and extant euryhaline *Lamprothamnium* Groves
990 (Charales) from Australia: Gyrogonite morphology and paleolimnological

991 significance. J Paleolimnol. 31(3):321–341.Ghetti P, Anadón P, Bertini A, Esu D,
992 Gliozzi E, Rook L, Soulié-Märsche I. 2002. The Early Messinian Velona Basin
993 (Siena, Central Italy): Paleoenvironmental and paleobiogeographical
994 reconstructions. Palaeogeogr Palaeoclimatol Palaeoecol. 187:1–33.

995 Gierlowski-Kordesch EH. 2010. Lacustrine carbonates. In: Alonso-Zarza AM, Tanner
996 LH, editors. Carbonates in Continental Settings. Facies, Environments and
997 Processes: Developments in Sedimentology, 61. Elsevier, Amsterdam: p. 1–101.

998 Gliozzi E, Rodriguez-Lazaro J, Nachite D, Martin-Rubio M, Bekkali R. 2005. An
999 overview of Neogene brackish leptocytherids from Italy and Spain:
1000 Biochronological and palaeogeographical implications. Palaeogeogr
1001 Palaeoclimatol Palaeoecol. 225:283–301.

1002 González-Pardos M. 2012. Carófitos del Mioceno inferior de la Formación Tudela
1003 (Cuenca del Ebro, Navarra). Master´s thesis, Universitat de Valencia: 69 p.

1004 Grambast L. 1962. Aperçu sur les Charophytes tertiaires du Languedoc et leur
1005 signification stratigraphique. C R Somm Séances Soc Géol Fr. 10:313–314.

1006 Grambast L, Grambast-Fessard N. 1954. Sur la position systématique de quelques
1007 charophytes tertiaires. Rev Gén Bot. 61:665–771.

1008 Grambast L, Paul P. 1965. Observations nouvelles sur la flore de charophytes du
1009 Stampien du bassin de Paris. Bull Soc Géol Fr. 7:239–247.

1010 Grambast L, Soulié-Märsche I. 1972. Sur l'ancienneté et la diversification des *Nitellopsis*
1011 (Charophytes). Paléobiol cont. 3:1–14.

1012 Groves J. 1916. On the name *Lamprothamnus* Braun. J Bot. 54:336–337.

1013 Guimerà J. 1992. Les fosses i depressions Neògenes. Història natural dels Països
1014 Catalans. Geologia 2. Enciclopedia Catalana, S.A. Barcelona: 548 p.

1015 Gusakov VA, Makhutova ON, Gladyshev MI. Golovatyuk LV, Zinchenko TD. 2021.
1016 Ecological role of *Cyprideis torosa* and *Heterocypris salina* (Crustacea,
1017 Ostracoda) in saline rivers of the Lake Elton basin: abundance, biomass,
1018 production, fatty acids. Zool Stud. 60:60–53.

1019 Holbourn A, Kuhnt W, Kochhann KGD, Andersen N, Sebastian Meier KJ. 2015. Global
1020 perturbation of the carbon cycle at the onset of the Miocene Climatic Optimum.
1021 Geology. 43(2):123–126. https://doi.org/10.1130/G36317.1

1022 Horn af Rantzien H. 1959. Morphological types and organ-genera of Tertiary Charophyte
1023 fructifications. Stockh Contrib Geol. 4:45–197.

1024 Huang RJ, Zhong ZQ, Nie YS. 1988. Early Tertiary Charophytes from the Dongpu
1025 region. In: Series on Stratigraphy and Paleontology of Oil and Gas bearing Areas
1026 in China. Research Institute of Exploration and Development, Zhongyuan
1027 Petroleum Exploration Bureau and Nanjing Institute of Geology and
1028 Paleontology, The Petroleum Industry Press, Beijing: 188 p.

1029 ICC (Institut Cartogràfic de Catalunya). ICGC - Vissir3 (icc.cat) (accessed 15 April
1030 2021).Janis CM. 1993. Tertiary mammal evolution in the context of changing
1031 climates, vegetation, and tectonic events. Annu Rev Ecol Syst. 24:467–500.

1032 Jovells-Vaqué S. 2020. Early Miocene cricetids from the Vallès- Penedès Basin
1033 (Catalonia): taxonomy, biostratigraphy and paleoecological implications. PhD
1034 Thesis, Universitat Autònoma de Barcelona, Bellaterra: 370 p.

1035 Jovells-Vaqué S, Casanovas-Vilar I. 2021. Dispersal and early evolution of the first
1036 modern cricetid rodents in Western Europe: new data from the Vallès-Penedès

1037 Basin (Catalonia). Comptes Rendus Palevol. 20(22):401–439.
1038 https://doi.org/10.5852/cr-palevol2021v20a22
1039 Julià de Agar JJ. 1991. Contribución al estudio de carófitos fósiles de la Cuenca Terciaria
1040 de Loranca (provincia de Cuenca, España). Coloquios de Paleontología 43:57–78.
1041 Katsuhara M, Tazawa M. 1986. Salt tolerance in *Nitellopsis obtusa*. Protoplasma
1042 135:155–161.
1043 Knobloch E. 1979. Fossil Charophyta from the Neogene and Holocene of Iraq. Věst Ústr
1044 Úst Geol. 54: 237–241.
1045 Korsch H. 2016. *Chara vulgaris*, In: Arbeitsgruppe Characeen Deutschlands, editors.
1046 Armleuchteralgen. Die Characeen Deutschlands. Springer Verlag, Heidelberg: p.
1047 379–387.
1048 Krause W. 1997. Charales (Charophyceae). Süsswasserflora von Mitteleuropa. Band 18.
1049 Gustav Fischer Verlag, Jena: 202 p.
1050 Leonhardi H Von. 1863. Über die böhmischen Characeen. Lothos 13:55–62.
1051 Lindley J. 1836. A Natural System of Botany. Longman, 2nd edition, London: 526 p.
1052 Linnæus C. 1753. Species plantarum, exhibentes plantas rite cognitas, ad genera relatas,
1053 cum differentiis specificis, nominibus trivialibus, synonymis selectis, loci
1054 natalibus, secundum sexuale digestas, vol. 2. Impensis Laurentii Salvii.
1055 Stockholm: p. 561–1.200.
1056 Liu JY. 1989. Cenozoic Paleobiota of the continental shelf of the East China Sea
1057 (Donghai). Geological Publishing House, Beijing: 324 p.
1058 Lu H, Luo Q. 1990. Fossil Charophytes from the Tarim Basin. Xinjiang. Series on
1059 Stratigraphy and Palaeontology of oil and gas bearing areas in China. Science and
1060 Technical Documents Publishing House, Beijing: 261 p.

1061 Ludwig K. 1987. Mikropaläontologische Hinweise für die autochthone Entstehung der
1062 miozänen Braunkohle im Becken von Teruel-Ademuz (NE- Spanien) Paläontol Z.
1063 61:17–27.

1064 Mädler K. 1952. Zur Taxonomie der Tertiären Charophyten. Geol Jahrb. 70:265–328.

1065 Mädler K. 1955. Charophyten aus dem Nordwestdeutschen Kimmeridge. Geol Jahrb. 67,
1066 1–46.

1067 Mädler K, Staesche U. 1979. Fossile Charophyten aus dem Könozoikum (Tertiär und
1068 Quartär) der Türkei. Geol Jahrb. B 33:81–157.

1069 Mannschreck B. 2003. *Chara hispida* (L.) Hartm. 1820. In: Schubert I, Blindow H,
1070 editors. Charophytes of the Baltic Sea. Gantner Verlag, Ruggell, Liechtenstein: p.
1071 107–112.

1072 Martín-Closas C. 1999. Epiphytic overgrowth of charophyte thalli by stromatolite-like
1073 structures and fungi in the Lower Cretaceous of the Iberian Ranges (Spain). Aust
1074 J Bot. 47: 305–313.

1075 Martín-Closas C, Ramos E. 2005. Palaeogene Charophytes of the Balearic Islands
1076 (Spain). Geol Acta. 3:39–58.

1077 Meisch C. 2000. Freshwater Ostracoda of Western and Central Europe. Süßwasserfauna
1078 von Mitteleuropa 8/3. Gustav Fischer, Stuttgart, 522 p.

1079 Meyen F. 1827. Beobachtung und Bemerkungen über die Gattung *Chara*. Linnaea
1080 2(1):55–81.

1081 Mennad A, Adaci M, Tabuce R, Martín-Closas C, Benyoucef M, Bensalah M, Otero O,
1082 Sarr R, Zaoui D. 2021. Découverte de charophytes et ostracodes de l'Yprésien
1083 inférieur dans les Monts des Ksour (Algérie): biostratigraphie et paléoécologie.
1084 Ann Paléontol. 107:102466.

1085 Migula W. 1897. Die Characeen, In: Rabenhorst L, editor. Kryptogamen-Flora von
1086 Deutschland, Oesterreich und der Schweiz. E. Kummer, Leipzig: 772 p.
1087 Miller KG, Browning JV, Schmelz WJ, Kopp RE, Mountain GS, Wright JD. 2020.
1088 Cenozoic sea-level and cryospheric evolution from deep-sea geochemical and
1089 continental margin records. Science Advances. 6(20): eaaz1346.
1090 https://doi.org/10.1126/sciadv.aaz1346
1091 Ortí F. 1990. Yesos de Vilobí (Mioceno). In: Ortí F, Salvany JM, editors. Formaciones
1092 evaporíticas de la Cuenca del Ebro y cadenas periféricas, y de la zona de Levante
1093 Barcelona, ENRESA: 306 p.
1094 Ortí F, Pueyo JJ. 1976. Yeso primario y secundario de depósito de Vilobí (província de
1095 Barcelona, España). Publicaciones del Instituto de Investigaciones Geológicas,
1096 Universidad de Barcelona 31:5–34.
1097 Ortíz JE, García-Cortés E, Colliga LA, Mansilla H, Torres T. 1998. Yacimientos de
1098 carofitas en la Depresión Intermedia (Cuenca, Guadalajara, España central).
1099 Geogaceta 23:115–118.
1100 Permanyer A. 1990. Sedimentologia i diagènesi dels esculls miocènics del Penedès.
1101 Arxius de les Seccions de Ciències, Institut d'Estudis Catalans 92: 321 p.
1102 Pukacz A, Boszke P, Pelechaty MJ, Raabe U. 2012. Comparative study of the oospore
1103 morphology of two populations of a rare species *Chara baueri* A. Braun in
1104 Cedynia (Poland) and Batzlow (Germany). Acta Soc Bot Pol. 81:131–136.
1105 Ramos-Guerrero E, Casas A, Pinto V, Agustí J. 1996. Estructura y relleno sedimentario
1106 de la semifosa Neógena de Vilanova (Garraf, Barcelona). Acta Geol Hisp. 29:93–
1107 106.

1108 Rasky K. 1945. Fossile Charophyten-Früchte aus Ungarn. Ungarischen
1109 Naturwissenschaftlichen Museums 2:1–75, 3 pl.

1110 Reichenbacher B, Schwarz J. 1997. Charophyten und Otolithen aus den Cyrenen-
1111 Schichten des nördlichen Alpenvorlandes. PalZ. 71:173–188.

1112 Roca E. 2001. The northwest Mediterranean (Valencia through, Gulf of Lyons and
1113 Liguro-Provençal basins): structure and geodynamic evolution. In: Ziegler PA,
1114 Cavazza W, Robertson AHF, Crasquin-Soleau S, editors. Peritehtyan rift/wrench
1115 basins and passive margins. Mém Mus Hist Natl Paris 186:671–706.

1116 Roca E, Guimerà J. 1992. The Neogene structure of the eastern Iberian margin: structural
1117 constraints on the crustal evolution of the Valencia through (Western
1118 Mediterranean). Tectonophysics 203:203–218.

1119 Roca E, Sans M, Cabrera L, Marzo M. 1999. Oligocene to Middle Miocene evolution of
1120 the Central Catalan margin (North-western Mediterranean). Tectonophysics 315:
1121 209–229.

1122 Ruprecht FJ. 1845. Distributio Cryptogamarum Vascularium in Imperio Rossico.
1123 Beiträge der Pflanzenkunde des Russischen Reiches 3: 56 p.

1124 Sanjuan J, Alqudah M. 2018. Charophyte flora from Miocene deposits of Zahle (Beeka
1125 Valley, Lebanon). Biostratigraphic, Palaeoenvironmental and
1126 Palaeobiogeographical implications. Geodiversitas 40 (10):195–209.

1127 Sanjuan J, Martín-Closas C. 2014. Taxonomy and palaeobiogeography of charophytes
1128 from the Upper Eocene-Lower Oligocene of the eastern Ebro basin (Catalonia,
1129 NE Spain). Geodiversitas 36 (3):385–420.

1130 Sanjuan J. Martín-Closas C. 2015. Biogeographic history of two Eurasiatic Cenozoic
1131 charophyte lineages. Aquat Bot. 120 (A):18–31.

1132 Sanjuan J, Vicente A, Flor-Arnau N, Monleón T, Cambra J, Martín-Closas C. 2017.
1133 Effects of light and temperature on *Chara vulgaris* gyrogonite productivity and
1134 polymorphism. Paleoenvironmental implications. Phycologia 56 (2):204–212.

1135 Sanz de Siria Catalán A. 1993. Datos sobre la paleoclimatología y paleoecología del
1136 Neógeno del Vallès-Penedès según las macrofloras halladas en la cuenca y zonas
1137 próximas. Paleontologia i Evolució 26–27:281–289.

1138 Sanz de Siria Catalán A. 1994. La evolución de las paleofloras en las cuencas cenozoicas
1139 catalanas. Acta Geol Hisp. 29:169–189.

1140 Schwarz J. 1997. Charophyten aus dem Tertiär des Oberrheingrabens (Mitteleozän-
1141 Untermiozän). Palaeontographica B 243:1–84.

1142 Schwarz J. Reichenbacher B. 1989. Die Charophytenflora der Kirchberger Schichten
1143 (Unter-Miozän). Geol Bavarica. 94:179–193.

1144 Smith GM. 1938. Botany. Algae and Fungi. Charophyceae. New York, McGraw Hill, 1:
1145 127 p.

1146 Soulié-Märsche I. 1978. Contributions a la Paléontologie du Miocéne Moyen continental
1147 du Bassin du Tage. IV-Charophytes-Póvoa de Santarém, Pęro Filho et Tremęs.
1148 Cięncias da Terra. Earth Sciences Journal 4:91–102.

1149 Soulié-Märsche I. 1982. Lac pléistocène du Fezzan (Libye). In: Le Shati (editions du
1150 centre national de la recherche scientifique). Marseille, France: p. 80–85.

1151 Soulié-Märsche I. 1989. Étude comparée de gyrogonites de charophytes actuelles et
1152 fossiles et phylogénie des genres actuels. Millau, Imprimerie des Tilleuls: 237 p.

1153 Soulié-Märsche I. 1991. Charophytes as lacustrine biomarkers during the Quaternary in
1154 North Africa. J Afr Earth Sci. 12 (1/2):341–351.

1155 Soulié-Märsche I. 1998. Fossil *Lamprothamnium papulosum* (Charophyta), a biomarker
1156 for seasonal rainfall in northern Mauritania. In: Heine K, editor. Paleoecology of
1157 Africa 25: p. 65–76.

1158 Soulié-Märsche I. 2007. Charophytes, indicators for low salinity phases in North sebkhet.
1159 J Afr Earth Sci. 51:69–76.

1160 Soulié-Märsche I. Martín-Closas, C. 2003. *Lychnothamnus barbatus* (Charophytes) from
1161 the Upper Miocene of La Cerdanya (Catalonia, Spain): taxonomic and
1162 palaeoecological implications. Acta Micropal Sinica. 20:156–165.

1163 Soulié-Märsche I, Gemayel P, Chaimanee Y, Suteethorn V, Jaeger JJ, Ducrocq S. 1997.
1164 *Nitellopsis* (Charophyta) from the Miocene of northern Thailand. Alcheringa
1165 21:141–156.

1166 Soulié-Märsche I, Benammi M, Gemayel P. 2002. Biogeography of living and fossil
1167 *Nitellopsis* (Charophyta) in relationship to new finds from Morocco. J Biogeogr.
1168 29:1703–1711.

1169 Soulié-Märsche I, Bieda S, Lafond R, Maley J, Baitoudji M, Vincent PM, Faure H. 2010.
1170 Charophytes as bio-indicators for lake level high stand at "Trou au Natron",
1171 Tibesti, Chad, during the Late Pleistocene. Glob Planet Change. 72 (4):334–340.

1172 Steinthorsdottir M, Coxall HK, Boer AM de, Huber M, Barbolini N, Bradshaw CD, Burls
1173 NJ, Feakins SJ, Gasson E, Henderiks J, Holbourn AE, Kiel S, Kohn J, Kürschner
1174 VM, Lear CH, Liebrand D, Kunt DJ, Mörs T, Pearson PN, Pound MJ, Stoll H,
1175 Strömberg E. 2020. The Miocene: the future of the past. Paleoceanogr
1176 Paleoclimatol. 36(4): e2020PA004037. https://doi.org/10.1029/2020PA004037.

1177 Straub EW. 1952. Mikropaläontologishe Untersuchungen im Tertiär zwischen Ehingen
1178 und Ulm an der Donau. Geol Jahrb. 66:433–524.

1179 Tang L, Di H. 1991. Fossil charophytes from Qaidam basin, Qinghai. Beijing: 220 p., 79
1180 pl. (in Chinese with abstract and table in English).

1181 Unger F. 1852. Iconographia plantarum fossilium. Denkschriften Akademie der
1182 Wissenschaften, Mathematisch-Naturwissenchaftliche Klasse, Wien 4: p. 73–118.

1183 Van Dam JA, Krijgsman W, Abels HA, García-Paredes I, López Guerrero P, Peláez-
1184 Campomanes P, Ventra D. 2014. Updated chronology for Middle to Late Miocene
1185 mammal sites of the Daroca area (Calatayud-Montalbán Basin, Spain). Geobios.
1186 47:325–334.

1187 Van der Meulen AJ, García-Paredes I, Álvarez Sierra MÁ, Van den Hoek Ostende LW,
1188 Hordijk K, Oliver A, Pélaez-Campomanes P. 2012. Updated Aragonian
1189 biostratigraphy: small mammal distribution and its implications for the Miocene
1190 European chronology. Geol Acta. 10:159–179.
1191 https://doi.org/10.1344/105.000001710

1192 Wallroth FG. 1833. Flora cryptogamia Germaniae. Pars posterior. Continens Algas et
1193 Fungos. In: Bluff MJ, Fingerhuth CA, editors. Compendium florae Germanicae.
1194 Sectio II plantae cryptogamicae sine cellulosae. Tomus IV: 923 p.

1195 Xinlun Z. 1978. Early Tertiary Charophytes from Coastal Region of Bohai. Nanjing
1196 Institute of Geology and Paleontology. Nanjing (in Chinese): 49 p.

1197 You Y, Huber M, Müller RD, Poulsen CJ, Ribbe J. 2009. Simulation of the Middle
1198 Miocene Climate Optimum. Geophys Res Lett. 36:L04702.
1199 doi:10.1029/2008GL036571.

1200 Zachos J, Pagani M, Sloan L, Thomas E, Billups K. 2001. Trends, rhythms, and
1201 aberrations in global climate 65 Ma to present. Science. 292(5517):686–693.
1202 https://doi.org/10.1126/science.1059412.

1203 Zachos JC, Dickens GR, Zeebe RE. 2008. An early Cenozoic perspective on greenhouse
1204 warming and carbon-cycle dynamics. Nature. 451(7176):279–283.
1205 https://doi.org/10.1038/nature06588.

1206

Figure captions

Figure 1. Geological map of the study area. Red stars represent the location of the three studied localities in the Vallès-Penedès and Vilanova i la Geltrú basins. V=Vilobí; E.C=els Casots; M.A= Mas de l´Alonso; P.G=el Pí Gros. Modified from ICC (2021).

Figure 2. Stratigraphic logs of the 4 studied localities. 1) els Casots (Subirats); 2) Vilobí del Penedès; 3) el Pí Gros (Vilanova i la Geltrú); 4) Mas de l´Alonso (Vilanova i la Geltrú).

Figure 3. Facies and microfacies from els Casots (Subirats). A–B. Field photos of the stratigraphic section. A. organic-claystones with pedogenetic features, see the location of the sample C4. B. limestone interval from where the samples C2 was extracted. C–H. Microphotographs of the limestone sample C2. C. Packstone of cyanobacterial crusts. D. subrounded oncoid. E. fragments of mollusk shells (m.s). F. detail of a mollusk shell. G. well-developed oncoid (Onc). H. detail of cyanobacterial crusts.

Figure 4. Field photos of the section at Vilobí del Penedès. A. laminated gypsarenite interval at the base of the section. B. gypsum (G) and claystone alternation at the base of the section, see the position of samples yielding charophytes V1, V3, and V4. C. Partially covered greenish claystones, see the position of the sample V5. D. Oyster bank at the top of the section.

Figure 5. Facies and microfacies from the el Pi Gros locality (Vilanova i la Geltrú). A.–B. Field photos of the stratigraphic section. A. general overview of the upper half section. B. facies showing a shallowing upward cycle from base to top; marly limestone (M), wackestone-packstone limestone (W-P. L), stromatolitic limestone (S.L) and bioturbated claystone (B.C). C–F. Microphotographs of the sample PG1. C. wackstone with gyrogonites (Gyr). D. Detail of a *Chara* gyrogonite showing the basal plate (B.P). E. wackestone–packstone with ostracods (ostr). F. wackestone–packstone with charophytes

1232 showing diagenetic dissolution. G–H. Microphotographs of PG4 sample, wackestone–
1233 packstone with ostracods (ostr), gyrogonites (gyr), and thalli.

1234 Figure 6. Fossil charophytes from the Vallès-Penedès and Vilanova i la Geltrú basins. A–
1235 D. *Sphaerochara ulmensis* from sample V6/7. A. apical view, IPS122528.1; B. lateral
1236 view, IPS122528.2; C. lateral views; IPS122528.3; D. basal view, IPS122528.4. E-I.
1237 *Sphaerochara ulmensis* from sample MA1, Mas de l´Alonso. E. apical view,
1238 IPS127516.1; F. lateral view, IPS127516.1; G. lateral view, IPS127516.2; H. lateral view,
1239 IPS127516.3; I. basal view, IPS127516.4; J–N. *Chara* cf. *vulgaris* from sample C4, els
1240 Casots. J. apical view, IPS127515.1; K. lateral view, IPS127515.2; L. lateral view,
1241 IPS127515.3; M. lateral view, IPS127515.4; N. basal view, IPS127515.5; O–R. *Chara*
1242 *molassica* var. *notata* from sample C4, els Casots. O. apical view, IPS127515.6; P. lateral
1243 view, IPS127515.7; Q. lateral view, IPS127515.8; R. basal view, IPS IPS127515.8; S–U.
1244 *Chara molassica* var. *notata* from sample V6/7, Vilobí del Penedès. S. apical view,
1245 IPS122528.5; T. lateral view, IPS122528.6; U. basal view, IPS122528.7

1246 Figure 7. Fossil charophyte assemblage from the Vallès-Penedès and Vilanova i la Geltrú
1247 basins (continued). A–H. *Chara* cf. *hispida* from sample PG2. A. lateral view,
1248 IPS127517.1; B. lateral view, IPS127517.2; C. lateral view, IPS127517.3; D. lateral view,
1249 IPS127517.4; E. apical view, IPS127517.5; F. apical view, IPS127517.6; G. basal view,
1250 IPS127517.7; H. basal view, IPS127517.8; I–M. *Chara* sp. from sample PG2. I. apical
1251 view, IPS127517.9; J. lateral view, IPS127517.10; K. lateral view, IPS127517.11; L.
1252 lateral view, IPS127517.12; M. basal view, IPS127517.13; N–U. *Lamprothamnium*
1253 *papulosum* from sample V5, Vilobí del Penedès. N. lateral view, IPS127514.1; O. lateral
1254 view, IPS127514.2; P. lateral view, IPS127514.3; Q. lateral view, IPS127514.4; R. apical
1255 view, IPS127514.5; S. apical view, IPS127514.6; T. basal view, IPS127514.7; U. basal
1256 view, IPS127514.8.

Figure 8. Fossil charophyte assemblage from the Vallès-Penedès and Vilanova i la Geltrú basins (continued). A–C. *Lychnothamnus barbatus* var. *antiquus* from sample V6/7, Vilobí del Penedès. A. apical view, IPS122528.8; B. lateral view, IPS122528.9; C. basal view, IPS122528.10; D–F. *Lychnothamnus* sp. from sample MA1, Mas de l´Alonso. D. apical view, IPS127516.5; E. lateral view, IPS127516.5; F. basal view, IPS127516.6; G–N. *Nitellopsis (Tectochara) merianii* from sample V6/7, Vilobí del Penedès. G. apical view, IPS122530.1; H. apical view, IPS122530.2; I. basal view, IPS122530.3; J. basal view, IPS122530.4; K. lateral view, IPS122530.5; L. lateral view, IPS122530.6; M. lateral view, IPS122530.7; N. lateral view, IPS122530.8; O–Q. *Nitellopsis* sp. from sample V6/7, Vilobí del Penedès. O. apical view, IPS122528.11; P. lateral view, IPS122528.11; Q. basal view. IPS122528.12.

Figure 9. Fossil ostracods and foraminifera from Vallès-Penedès and Vilanova i la Geltrú basins. A–D. *Heterocypris salina* from sample PG2, el Pi Gros locality. A. external view of a right valve, IPS127517.14; B. internal view of a right valve, IPS127517.15; C. dorsal view of carapace, IPS127517.16; D. ventral view of carapace, IPS127517.17; E–J. ?*Leptocythere* gr. *L. psammophila* from sample PG2, el Pi Gros locality. E. external view of a left valve, IPS127517.18; F. external view of a left valve, IPS127517.19; G. external view of a right valve, IPS127517.20; H. opened carapaces from the ventral view, IPS127517.21; I. dorsal view of carapace, IPS127517.22; J. ventral view of carapace, IPS127517.23; K–M. *Ammonia* sp. from sample C4, els Casots. K. umbilical view, IPS127515.9; L. umbilical view, IPS127515.10; M. spiral view, IPS127515.11.

Figure 10. Palaeoenvironmental model showing the distribution of the charophyte taxa and the distinguished depositional environments in the Vallès-Penedès and Vilanova i la Geltrú basins. Note that this is not a palaeoenvironmental reconstruction, as the Vallès-Penedès sites date back to the Langhian while those from the Vilanova i la Geltrú date

1282 back to the Serravallian. The figure is meant to illustrate the range of wetland
1283 environments occurring in these coastal basins during the Middle Miocene.

1284 Table 1. List of microfossils and their relative abundances based on a semi-quantitative
1285 visual estimation.

1286 Table 2 (in supplementary data). Biometric measurements of the studied charophyte
1287 samples from the Middle Miocene deposits of the E Vallès-Penedès and Vilanova i la
1288 Geltrú basins.

Figure 1

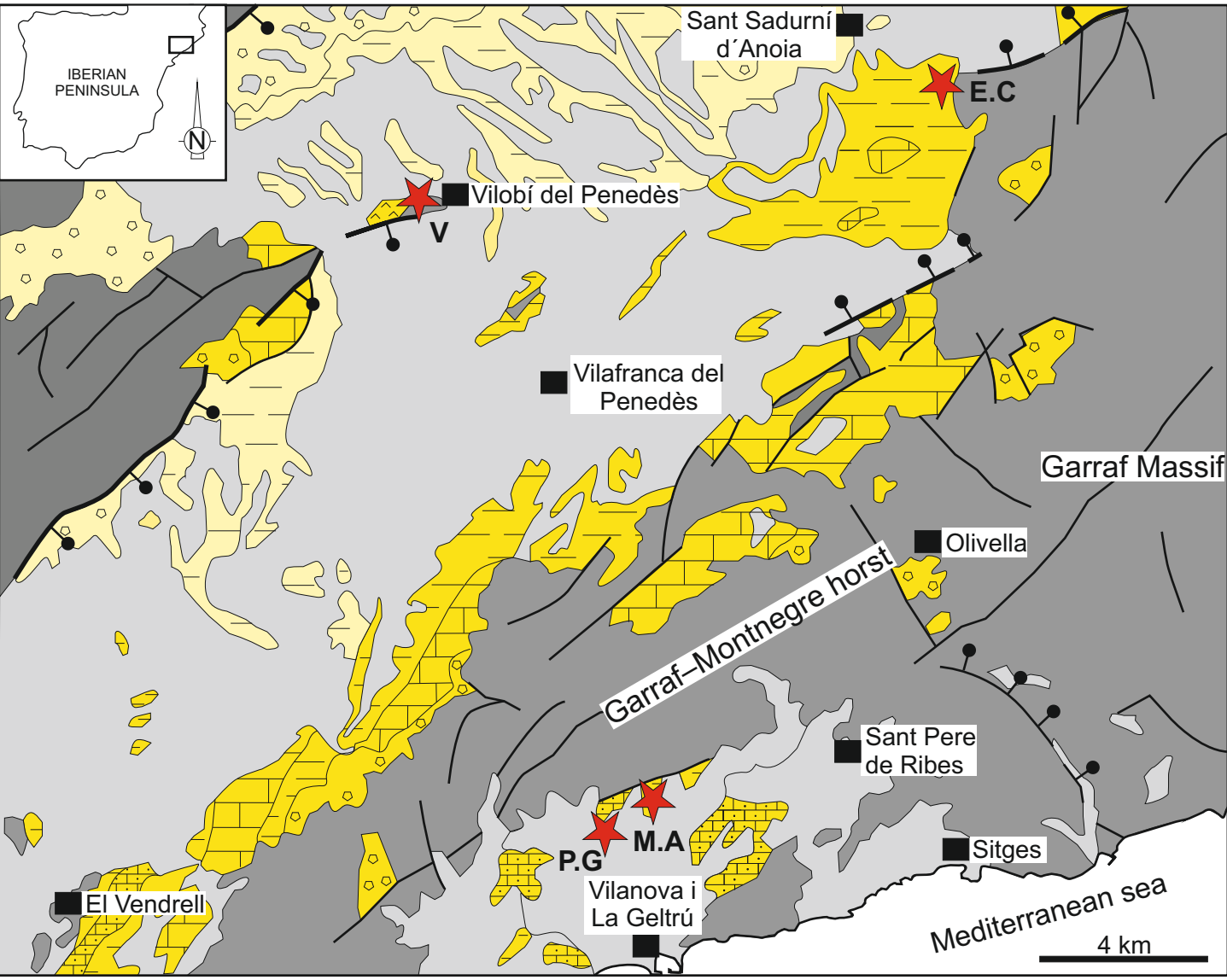

Legend

- Village
- Section location
- Major normal faults
- Minor faults
- Quaternary (fluvial, alluvial and beach deposits)
- Early Miocene (comglomerate and coarse sandstone)
- Early Miocene (marls and mudstone)
- Early Miocene (reefal limestone)
- Early/Middle Miocene (bioclastic limestone)
- Early Miocene (gypsum)
- Middle/Late Miocene (comglomerate)
- Middle/Late Miocene (marls and mudstone)
- Jurassic and Cretaceous rocks (limestone)

Figure 2

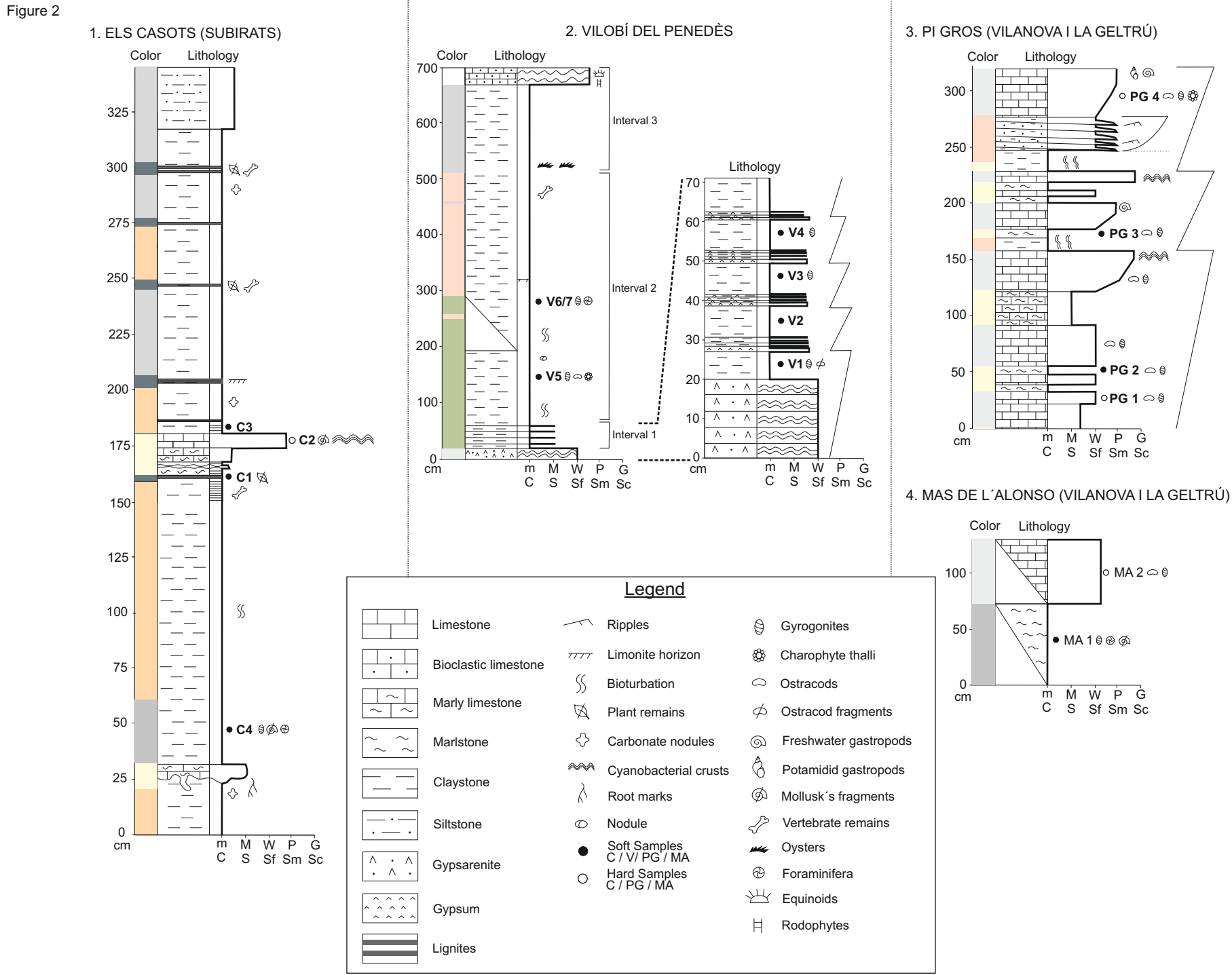
1. ELS CASOTS (SUBIRATS)
Color
Lithology
325
300
275
250
225
200
175
150
125
100
75
50
25
0
cm
C3
C2
C1
C4
m C
M S
W Sf
P Sm
G Sc
2. VILOBÍ DEL PENEDÈS
Color
Lithology
700
600
500
400
300
200
100
0
cm
Interval 3
Interval 2
Interval 1
V6/7
V5
Lithology
70
60
50
40
30
20
10
0
V4
V3
V2
V1
3. PI GROS (VILANOVA I LA GELTRÚ)
Color
Lithology
300
250
200
150
100
50
0
cm
PG 4
PG 3
PG 2
PG 1
4. MAS DE L´ALONSO (VILANOVA I LA GELTRÚ)
Color
Lithology
100
50
0
cm
MA 2
MA 1
Legend
Limestone
Bioclastic limestone
Marly limestone
Marlstone
Claystone
Siltstone
Gypsarenite
Gypsum
Lignites
Ripples
Limonite horizon
Bioturbation
Plant remains
Carbonate nodules
Cyanobacterial crusts
Root marks
Nodule
Soft Samples C / V/ PG / MA
Hard Samples C / PG / MA
Gyrogonites
Charophyte thalli
Ostracods
Ostracod fragments
Freshwater gastropods
Potamidid gastropods
Mollusk´s fragments
Vertebrate remains
Oysters
Foraminifera
Equinoids
Rodophytes

Figure 3

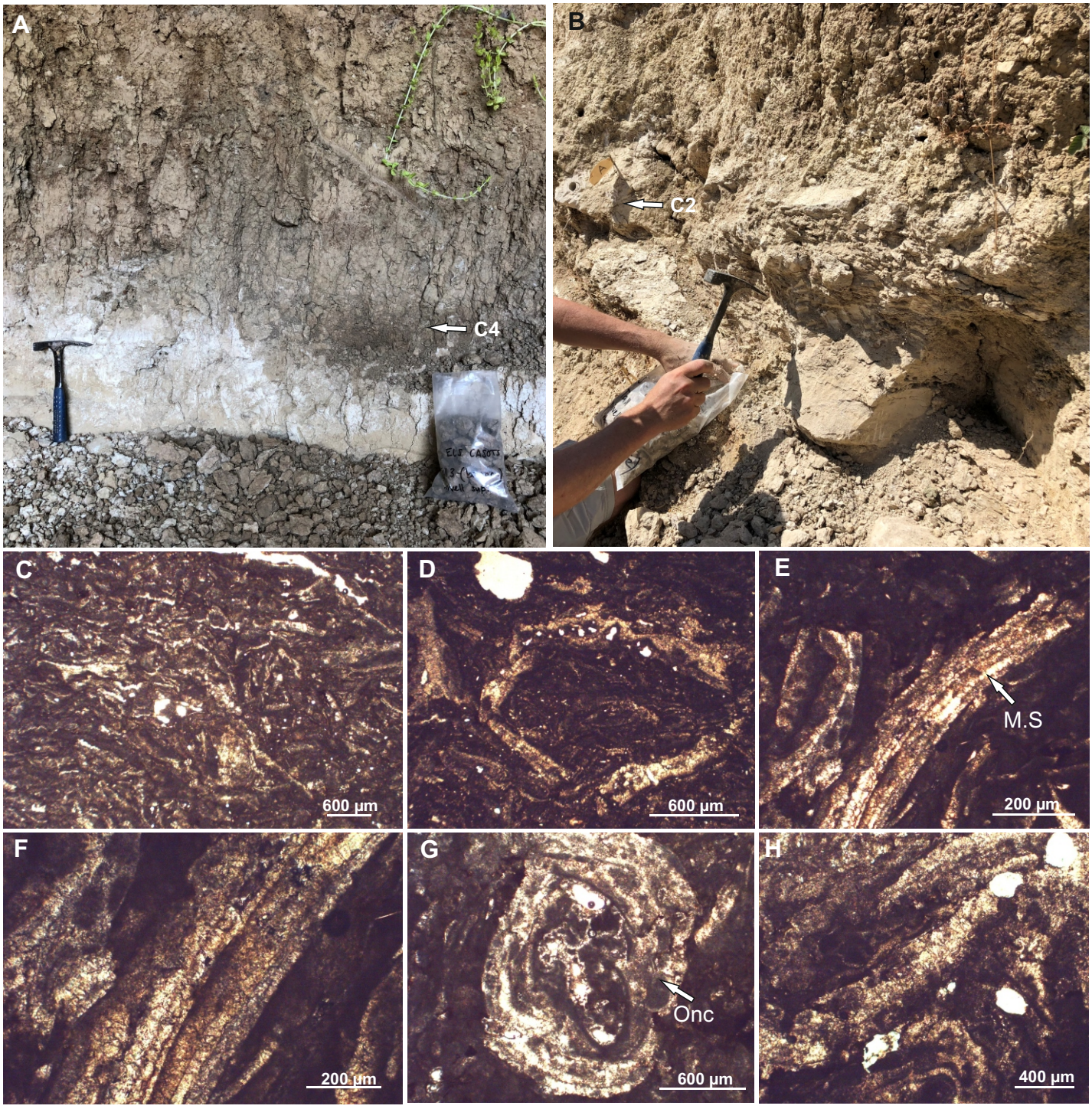

Figure 4

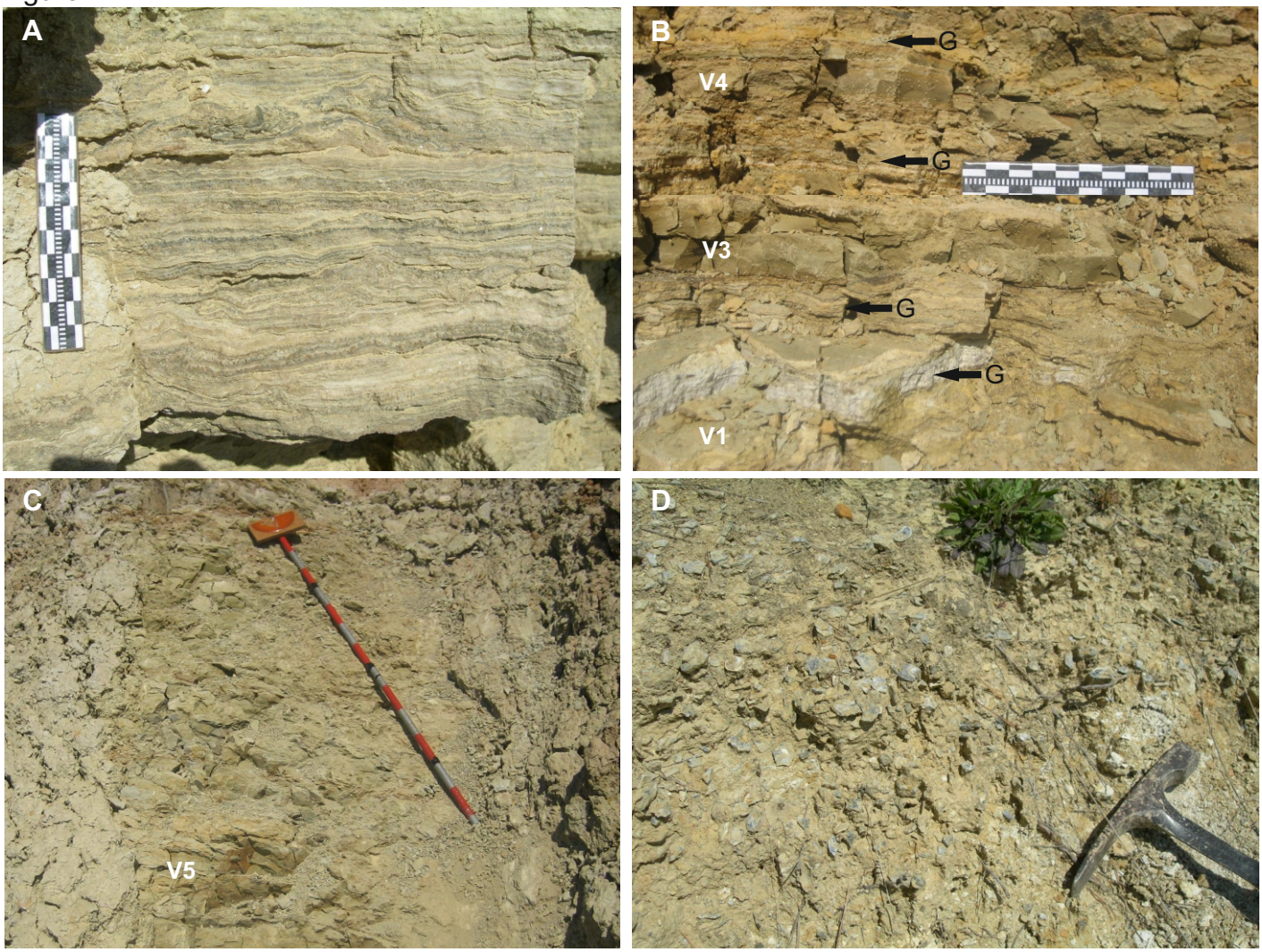

Figure 5

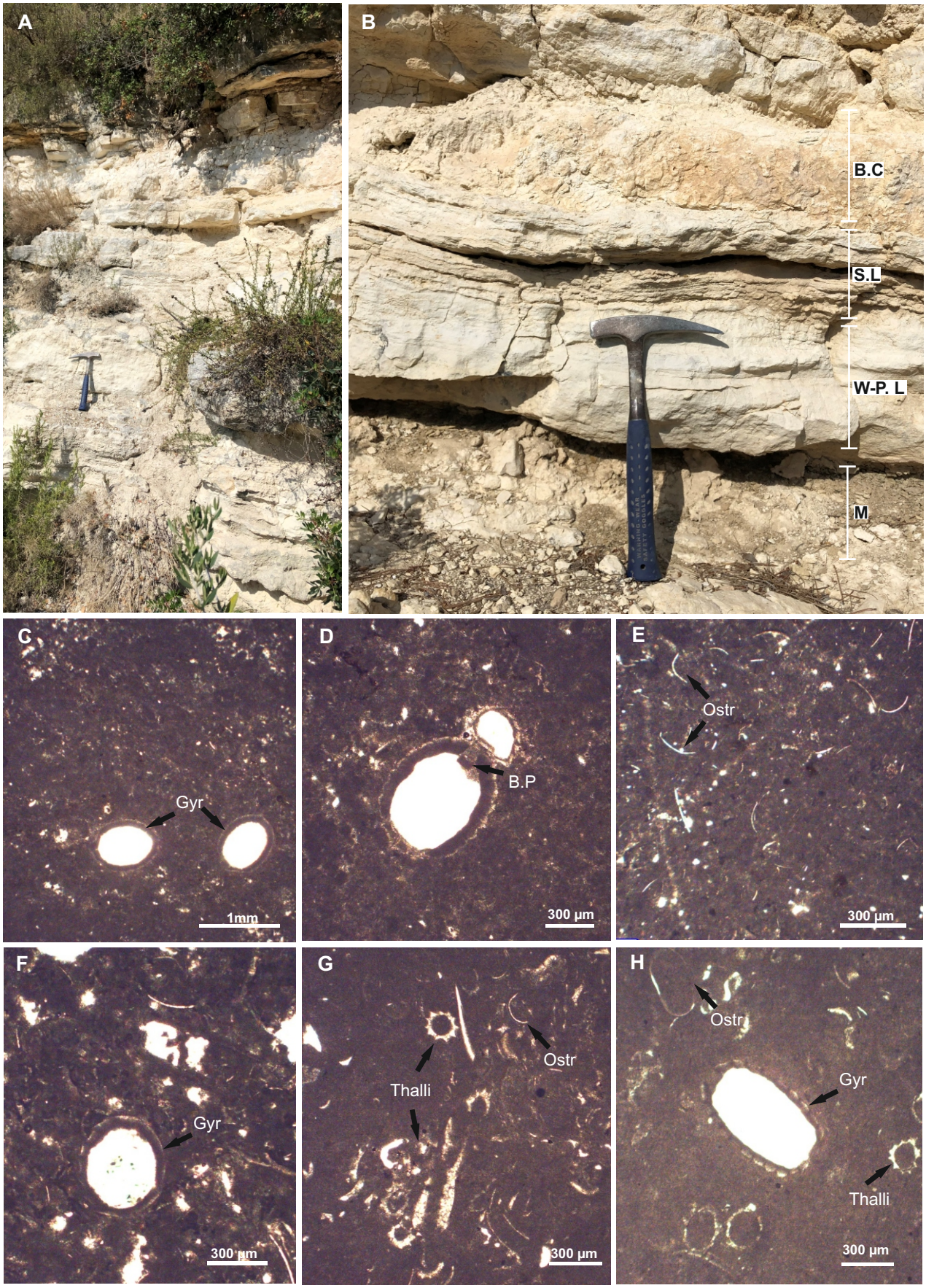
A
B
B.C
S.L
W-P. L
M
C
Gyr
1mm
D
B.P
300 µm
E
Ostr
300 µm
F
Gyr
300 µm
G
Thalli
Ostr
300 µm
H
Ostr
Gyr
Thalli
300 µm

Figure 6

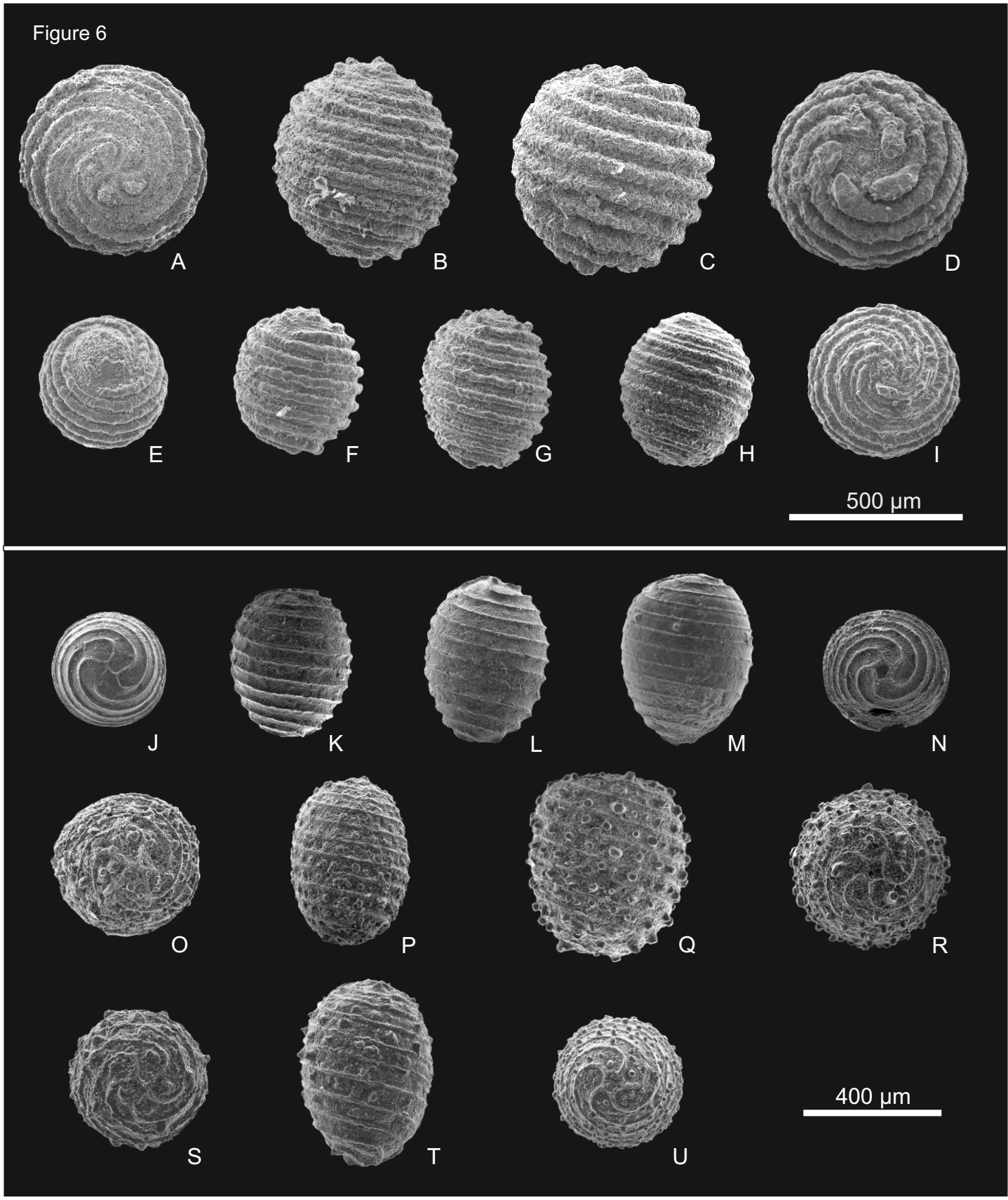

Figure 7

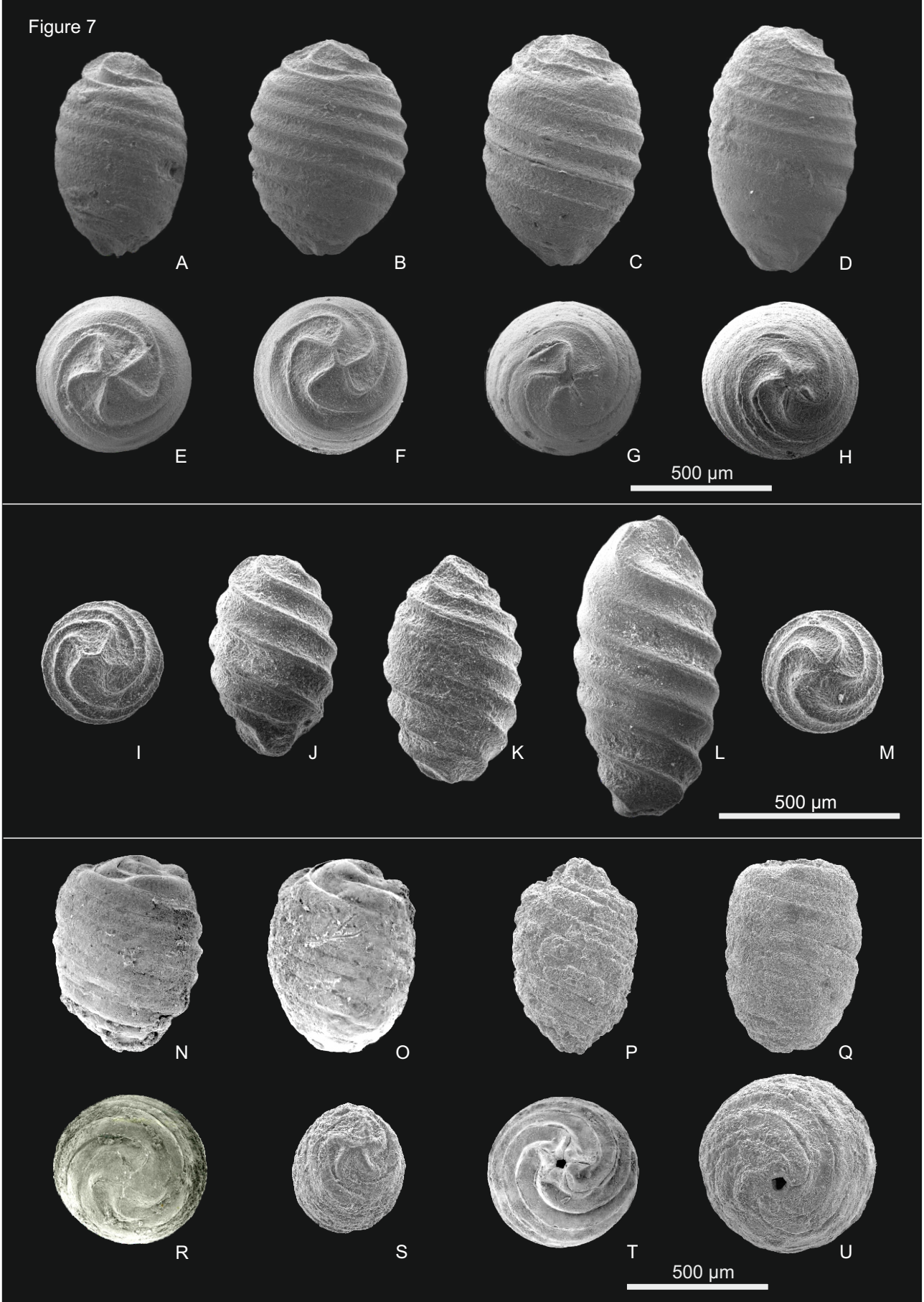

Figure 8

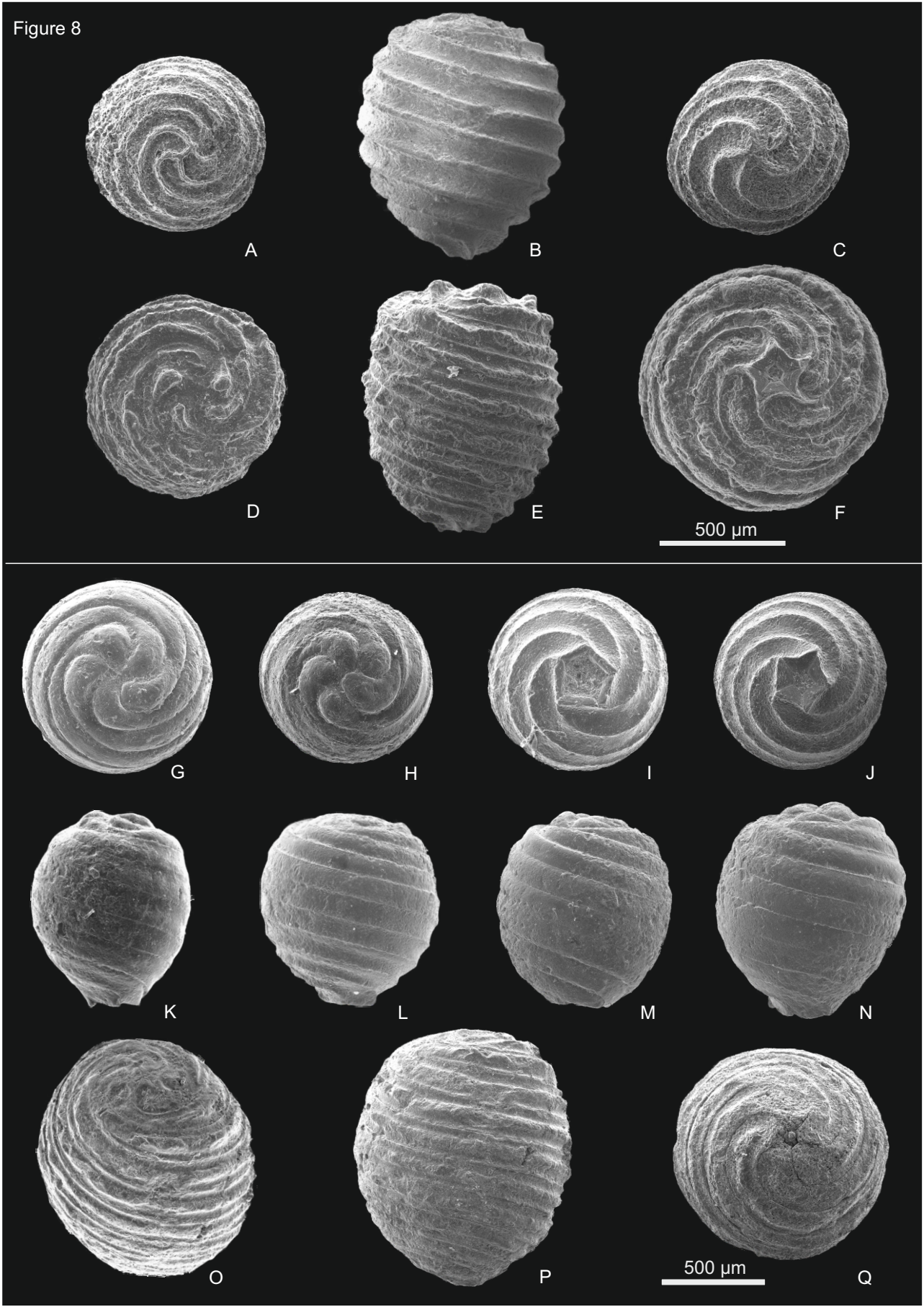

Figure 9

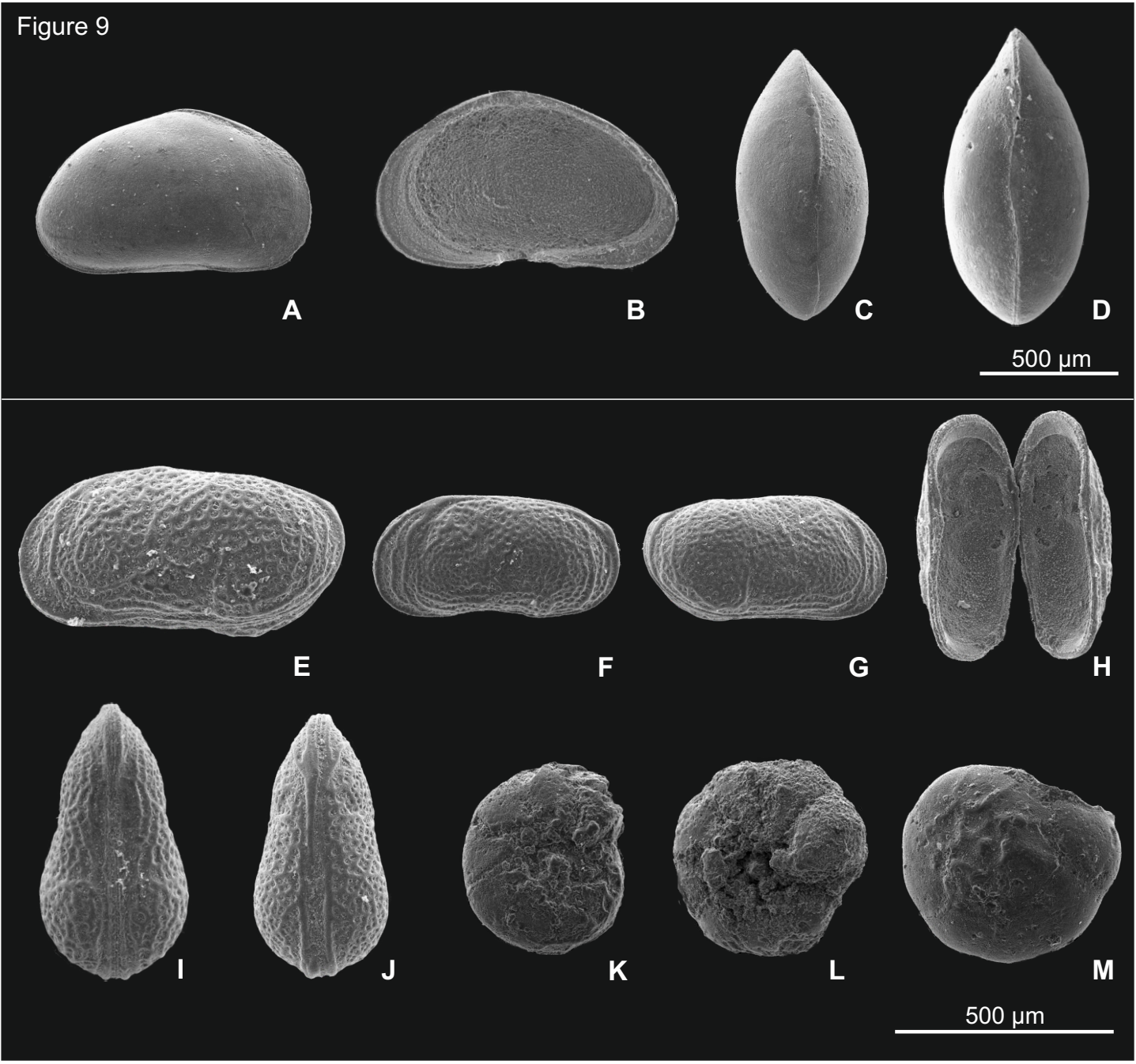

Figure 10

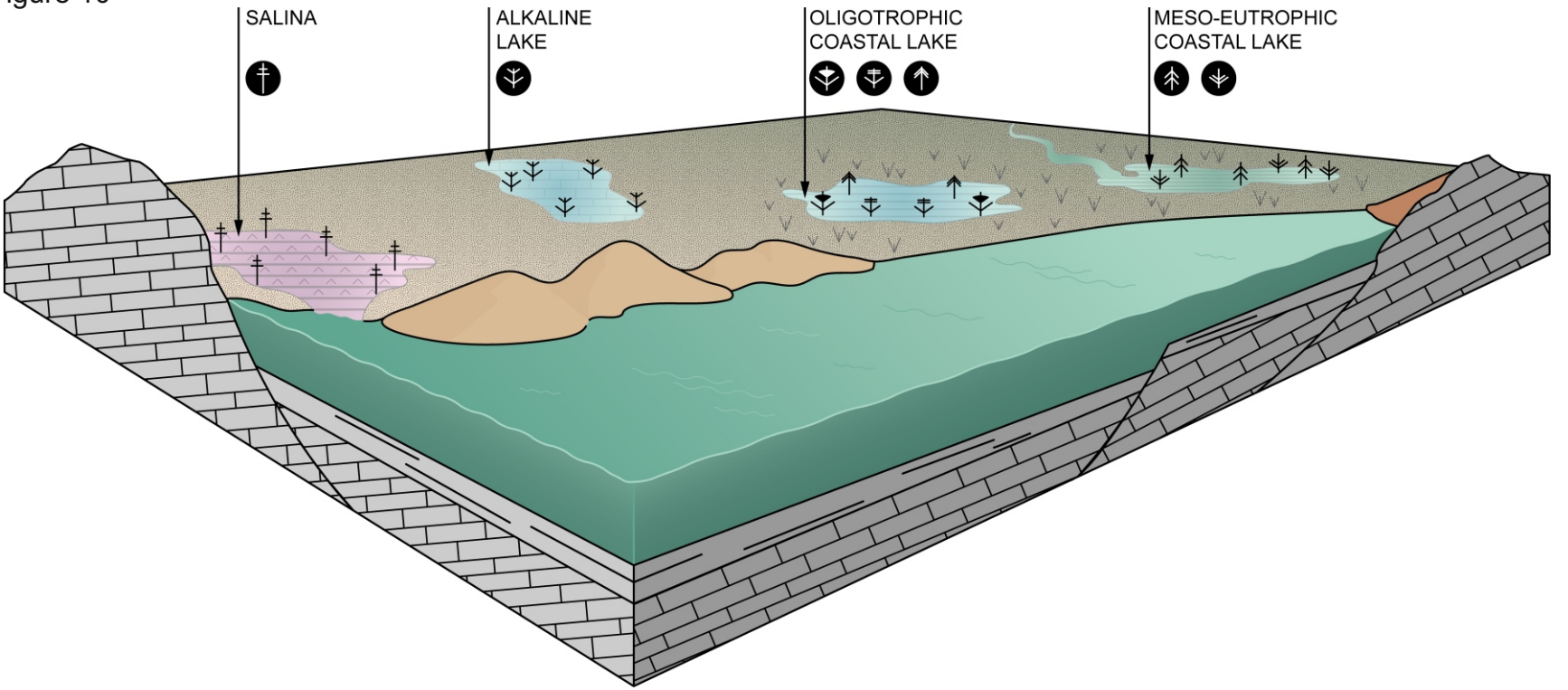
SALINA
ALKALINE LAKE
OLIGOTROPHIC COASTAL LAKE
MESO-EUTROPHIC COASTAL LAKE
Helophytic plants
Lamprothamnium papulosum
Chara molassica var. notata
Chara cf. vulgaris
Chara cf. hispida
Sphaerochara ulmensis
Lychnothamnus barbatus var. antiquus
Nitellopsis merianii

Table 1

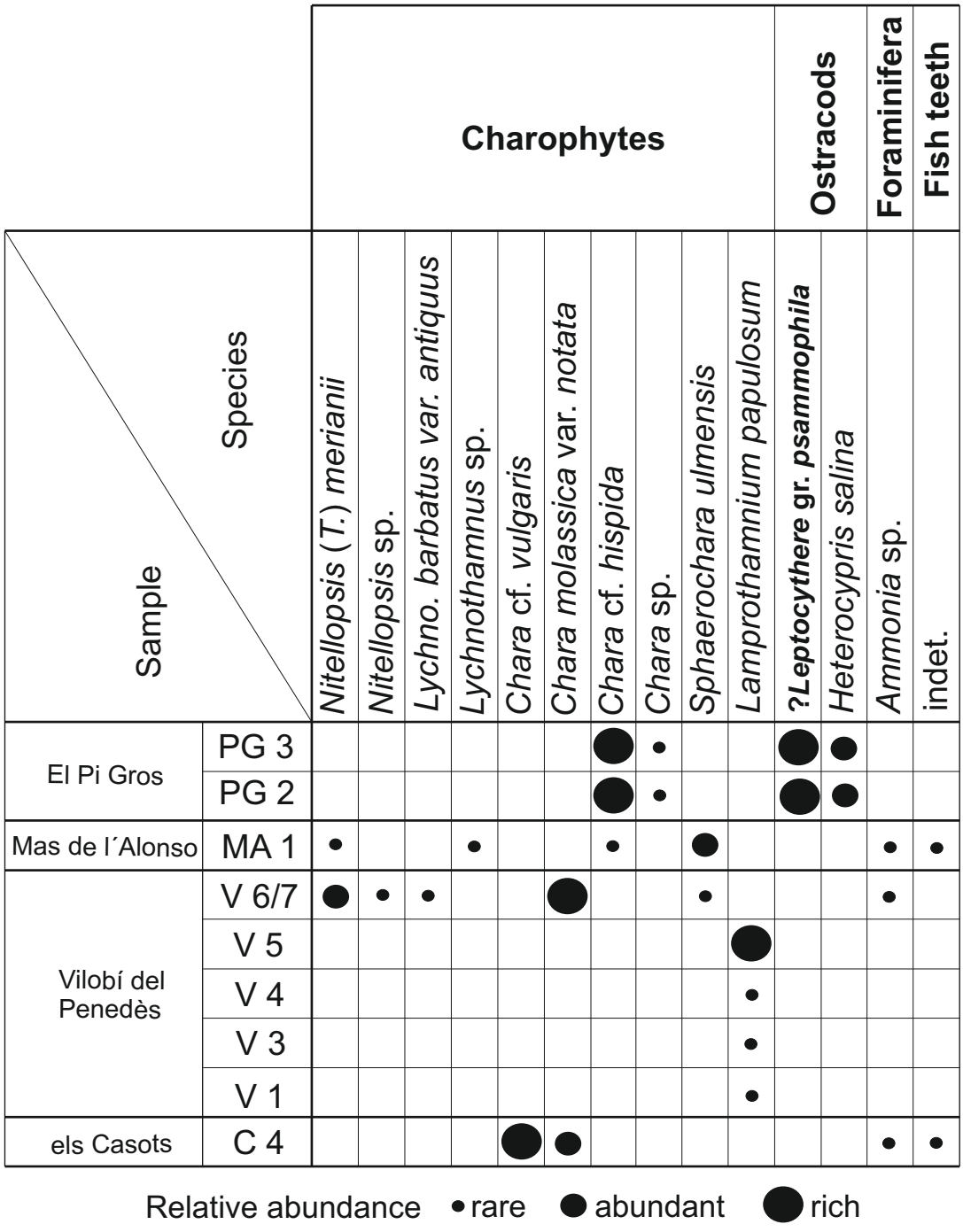
Charophytes
Ostracods
Foraminifera
Fish teeth
Sample
Species
Nitellopsis (T.) meriannii
Nitellopsis sp.
Lychno. barbatus var. antiquus
Lychnothamnus sp.
Chara cf. vulgaris
Chara molassica var. notata
Chara cf. hispida
Chara sp.
Sphaerochara ulmensis
Lamprothamnium papulosum
?Leptocythere gr. psammophila
Heterocypris salina
Ammonia sp.
indet.
El Pi Gros
PG 3
PG 2
Mas de l´Alonso
MA 1
Vilobí del Penedès
V 6/7
V 5
V 4
V 3
V 1
els Casots
C 4
Relative abundance
rare
abundant
rich

Table 2 (supplementary data).

H=gyrogonite height, µm
W=gyrogonite width, µm
C.N=convolution number in lateral view
S.C.H=spiral cell height, µm
ISI=Isopolarity index. H/W x 100

ELS CASOTS

Chara molassica var. *notata.* Sample C4

H	W	C.N	S.C.H	ISI	
550	439	10	56	125	
491	369	11	44	133	
641	404	11	54	159	
538	418	11	44	129	
555	408	11	50	136	mean
491	369	10	44	125	min
641	439	11	56	159	max

Chara cf. *vulgaris.* Sample C4

H	W	C.N	S.C.H	ISI
419	335	11	31	125
475	375	12	53	127
454	325	10	42	140
501	305	10	33	164
504	391	12	43	129
520	365	11	38	142
486	347	11	49	140
435	386	10	53	113
513	430	11	43	119
483	359	10	42	135
401	289	12	42	139
455	371	11	52	123
451	390	13	51	116
552	359	11	38	154
482	384	11	46	126
460	402	11	44	114
533	414	13	45	129
529	429	12	49	123
495	356	13	41	139
473	357	11	49	132
584	406	12	54	144
446	360	11	41	124
414	370	10	45	112
437	355	11	37	123
382	336	12	38	114
468	374	11	44	125

Table 2 (supplementary data).

456	293	12	40	156	
465	359	10	41	130	
481	375	10	54	128	
442	377	10	60	117	
470	299	10	48	157	
444	346	11	45	128	
456	333	10	39	137	
481	350	10	33	137	
474	301	11	42	157	
378	323	11	48	117	
435	345	12	43	126	
487	352	12	37	138	
468	323	11	48	145	
543	357	10	53	152	
492	330	10	57	149	
426	256	10	39	166	
449	325	12	40	138	
428	334	11	37	128	
386	319	10	39	121	
470	347	10	45	135	
467	361	12	46	129	
501	333	12	43	150	
419	325	10	42	129	
421	363	12	46	116	
466	352	11	44	133	mean
378	256	10	31	112	min
584	430	13	60	166	max

VILOBÍ DEL PENEDÈS					
Chara molassica var. *notata.* Sample V6/7					
H	W	C.N	S.C.H	ISI	
488	320	11	53	153	
570	402	11	56	142	
542	383	10	68	142	
517	331	9	60	156	
498	411	10	52	121	
544	389	9	71	140	
531	368	10	51	144	
557	384	9	72	145	
547	368	11	51	149	
468	333	10	58	141	
523	386	10	57	135	
478	398	10	64	120	
509	344	9	60	148	
558	367	10	50	152	
451	416	8	69	108	

Table 2 (supplementary data).

599	407	10	60	147	
508	375	9	59	135	
513	412	8	53	125	
438	336	10	51	130	
519	407	10	61	128	
527	398	9	69	132	
580	363	11	46	160	
513	407	9	52	126	
480	353	10	47	136	
551	415	9	69	133	
536	401	9	61	134	
452	343	9	66	132	
491	347	10	54	141	
527	375	11	57	141	
584	362	12	51	161	
517	396	9	69	131	
520	377	10	59	138	mean
599	416	12	72	161	max
438	320	8	46	108	min

Sphaerochara ulmensis. Sample V6/7

H	W	C.N	S.C.H	ISI	
590	576	10	62	102	
630	619	9	73	102	
652	564	9	84	116	
623	569	9	74	109	
596	582	9	79	102	
622	567	10	73	110	
614	514	10	64	119	
571	514	10	63	111	
607	578	10	71	105	
612	565	10	71	109	mean
652	619	10	84	119	max
571	514	9	62	102	min

Nitellopsis (Tectochara) merianii. Sample V6/7

H	W	number conv.	conv H	ISI	
986	863	9	130	114	
964	856	9	161	113	
969	790	8	149	123	
1035	767	9	130	135	
907	832	8	145	109	
781	656	8	104	119	
914	774	8	170	118	
1004	786	7	158	128	
1120	957	8	171	117	

Table 2 (supplementary data).

997	818	7	183	122	
998	856	7	145	117	
1079	914	8	141	118	
947	867	8	149	109	
922	886	7	179	104	
933	852	7	158	110	
843	786	9	107	107	
894	810	7	137	110	
958	866	8	130	111	
1023	815	7	123	126	
804	676	7	104	119	
955	811	7	158	118	
854	709	7	118	120	
959	847	7	131	113	
1036	904	8	131	115	
1066	913	9	181	117	
1004	865	8	152	116	
899	816	7	130	110	
943	813	7	164	116	
988	838	7	139	118	
928	697	7	131	133	
951	878	9	114	108	
1060	914	9	134	116	
914	841	8	129	109	
981	836	9	122	117	
900	740	8	140	122	
958	824	8	141	116	mean
1120	957	9	183	135	max
781	656	7	104	104	min

Nitellopsis sp. Sample V6/7

H	W	C.N	S.C.H	ISI	
1335	1053	8	164	127	
1243	1048	9	146	119	
1289	1051	9	155	123	mean

Lychnothamnus barbatus var. *antiquus*. Sample V6/7

H	W	C.N	S.C.H	ISI	
934	787	10	113	119	
726	600	9	107	121	
974	812	10	153	120	
878	733	10	124	120	mean

Lamprothamnium papulosum. Sample V5

H	W	C.N	S.C.H	ISI	
592	464	10	88	128	

Table 2 (supplementary data).

639	506	10	85	126
583	491	9	85	119
700	486	11	70	144
632	504	10	75	125
653	490	10	85	133
608	460	10	63	132
663	542	11	78	122
638	495	11	85	129
634	459	10	86	138
613	488	11	85	126
653	484	10	82	135
598	446	11	68	134
581	486	10	68	120
638	499	9	87	128
627	442	10	73	142
658	455	10	67	145
591	458	9	78	129
650	507	9	73	128
583	478	9	94	122
569	431	9	87	132
639	455	10	88	140
604	479	9	89	126
628	528	9	76	119
657	422	8	100	156
666	452	8	73	147
606	460	8	76	132
610	538	8	93	113
651	499	9	84	130
640	460	9	96	139
619	478	9	87	129
649	505	9	95	129
617	467	9	89	132
639	457	8	85	140
637	510	8	70	125
636	447	8	85	142
625	444	8	71	141
589	441	9	95	134
620	484	10	92	128
586	422	9	87	139
591	413	8	85	143
629	433	9	67	145
690	436	9	72	158
610	455	9	75	134
616	462	11	76	133
599	460	9	78	130
663	373	9	73	178

Table 2 (supplementary data).

631	511	10	90	123	
661	448	8	75	148	
638	501	9	84	127	
601	474	8	89	127	
571	391	8	95	146	
649	506	10	62	128	
677	459	9	73	147	
622	459	9	78	136	
701	528	9	81	133	
682	519	8	86	131	
711	452	9	86	157	
682	480	9	96	142	
585	348	8	75	168	
631	469	9	81	135	mean
711	542	11	100	178	max
569	348	8	62	113	min

MAS DE L´ALONSO–EL PI GROS

Chara cf. *hispida*. Sample PG2

H	W	C.N	S.C.H	ISI
783	540	10	80	145
783	540	9	88	145
783	513	10	104	153
783	540	10	88	145
783	567	9		138
567	378	8		150
810	540	10		150
621	432	10		144
621	459	9		135
810	540	10		150
864	567	8		152
594	378	8		157
783	540	10		145
756	486	9		156
810	567	10		143
810	540	11		150
648	405	10		160
540	432	12		125
594	405			147
810	567			143
675	351			192
810	540			150
756	567			133
729	540			135
756	540			140
729	513			142

Table 2 (supplementary data).

729	513	142
756	540	140
540	405	133
783	540	145
810	567	143
675	486	139
648	405	160
702	540	130
810	540	150
702	432	163
891	439	203
648	567	114
675	540	125
540	432	125
648	432	150
810	540	150
567	405	140
702	567	124
724	540	134
756	513	147
702	432	163
756	513	147
648	405	160
837	540	155
783	540	145
702	486	144
756	459	165
783	486	161
675	513	132
810	567	143
783	540	145
783	540	145
648	405	160
621	405	153
702	486	144
810	567	143
756	513	147
540	351	154
783	540	145
702	486	144
594	540	110
783	567	138
810	513	158
810	513	158
621	486	128
756	459	165

Table 2 (supplementary data).

594	432			138	
756	513			147	
567	432			131	
594	405			147	
837	405			207	
810	621			130	
756	486			156	
783	567			138	
687	540			127	
756	486			156	
729	486			150	
729	513			142	
702	540			130	
810	540			150	
702	540			130	
783	567			138	
540	378			143	
675	540			125	
810	540			150	
810	540			150	
729	540			135	
621	486			128	
756	540			140	
810	459			176	
726	467			155	
774	548			141	
806	572			141	
854	516			166	
726	500	9,6	90	145	mean
891	621			207	max
540	351			110	min

Chara sp. Sample PG2

H	W	C.N	S.C.H	ISI	
612	350	6	100	175	
625	387	7	75	161	
825	400	7	112	206	
687	379	7	96	181	mean

Sphaerochara ulmensis. Sample MA1

H	W	C.N	S.C.H	ISI	
477	431	9	50	111	
433	407	10	41	106	
413	330	10	39	125	
413	378	9	43	109	
446	385	10	43	116	

Table 2 (supplementary data).

398	374	9	53	106	
447	379	9	44	118	
447	363	9	54	123	
449	409	10	61	110	
446	410	10	52	109	
418	375	10	43	111	
447	421	10	66	106	
442	404	9	45	109	
426	383	9	60	111	
466	402	9	53	116	
460	417	9	57	110	
410	388	9	62	106	
437	397	10	48	110	
424	402	10	57	105	
436	406	9	63	107	
421	375	9	62	112	
453	378	10	54	120	
437	390	9	51	112	
437	391	9	52	112	mean
477	431	10	66	125	max
398	330	9	39	105	min

Lychnothamnus sp. Sample MA1

H	W	C.N	S.C.H	ISI
1022	777	8	70	131